Published in final edited form as:

Dev Cell. 2021 August 09; 56(15): 2237–2251.e6. doi:10.1016/j.devcel.2021.06.021.

Specialized endothelial tip cells guide neuroretina vascularization and blood-retina-barrier formation

Georgia Zarkada[1], **Joel P. Howard**[2,5], **Xue Xiao**[2,3,5], **Hyojin Park**[1], **Mathilde Bizou**[2,3], **Severine Leclerc**[2], **Steffen E. Künzel**[1], **Blanche Boisseau**[2], **Jinyu Li**[1], **Gael Cagnone**[2], **Jean Sebastien Joyal**[2], **Gregor Andelfinger**[2], **Anne Eichmann**[1,4,*], **Alexandre Dubrac**[2,3,6,*]

[1]Yale Cardiovascular Research Center, Section of Cardiovascular Medicine, Department of Internal Medicine, Yale University School of Medicine, New Haven, CT 06511, USA

[2]Centre de Recherche, CHU St. Justine, Montréal, QC H3T 1C5, Canada

[3]Département de Pathologie et Biologie Cellulaire, Université de Montréal, Montréal, QC H3T 1J4, Canada

[4]Department of Cellular and Molecular Physiology, Yale University School of Medicine, New Haven, CT 06520, USA

[5]These authors contributed equally

[6]Lead contact

SUMMARY

Endothelial tip cells guiding tissue vascularization are primary targets for angiogenic therapies. Whether tip cells require differential signals to develop their complex branching patterns remained unknown. Here, we show that diving tip cells invading the mouse neuroretina (D-tip cells) are distinct from tip cells guiding the superficial retinal vascular plexus (S-tip cells). D-tip cells have a unique transcriptional signature, including high TGF-β signaling, and they begin to acquire blood-retina barrier properties. Endothelial deletion of TGF-β receptor I (*Alk5*) inhibits D-tip cell identity acquisition and deep vascular plexus formation. Loss of endothelial ALK5, but not of the canonical SMAD effectors, leads to aberrant contractile pericyte differentiation and hemorrhagic vascular malformations. Oxygen-induced retinopathy vasculature exhibits S-like tip cells, and *Alk5* deletion impedes retina revascularization. Our data reveal stage-specific tip cell heterogeneity as a requirement for retinal vascular development and suggest that non-

*Correspondence: anne.eichmann@yale.edu (A.E.), alexandre.dubrac@umontreal.ca (A.D.).

AUTHOR CONTRIBUTIONS

G.Z., A.E., and A.D. designed and analyzed all experiments. G.Z., A.D., H.P., M.B., B.B., J.L., and S.E.K. performed experiments. J.P.H. and G.C. performed computational analysis. X.X. set up retinal cell isolation protocols and performed isolations. S.L. performed 10X Genomics single-cell sequencing. J.S.J. and G.A. provided equipment and advice and discussed results. G.Z., A.E., and A.D. wrote the manuscript. A.E. and A.D. conceptualized the study. All authors discussed results and commented on the manuscript.

SUPPLEMENTAL INFORMATION

Supplemental information can be found online at https://doi.org/10.1016/j.devcel.2021.06.021

DECLARATION OF INTERESTS

The authors declare no competing interests.

canonical-TGF-β signaling could improve retinal revascularization and neural function in ischemic retinopathy.

Graphical Abstract

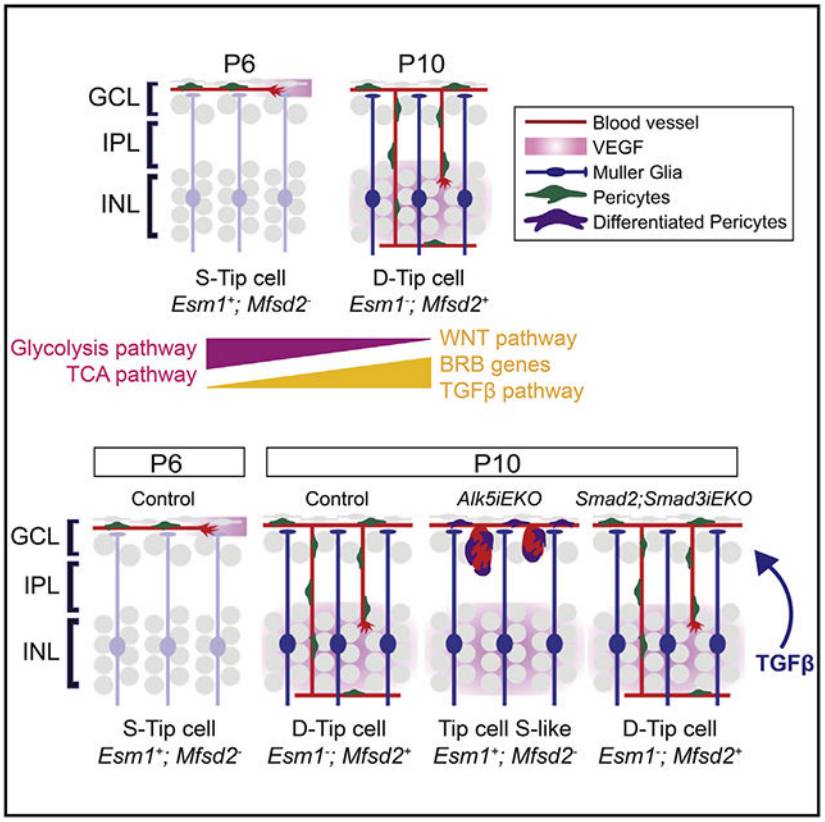

In brief

As initiators of neovascularization, endothelial tip cells are primary targets for angiogenic therapies. Zarkada et al. use scRNA sequencing to identify a TGF-β-dependent tip cell population that promotes neuroretina vascularization and could be targeted therapeutically to promote revascularization in retinopathies.

INTRODUCTION

Endothelial tip cells are specialized cells at the extremity of newly formed capillaries that extend filopodia and guide capillary outgrowth (Potente et al., 2011; Adams and Eichmann, 2010). They initiate branching morphogenesis and are selected via mechanisms conserved between tubular epithelial systems. For example, tip cells in the *Drosophila* trachea epithelium are selected by high FGF signals, while endothelial tip cells respond to high levels of VEGF (Gerhardt and Betsholtz, 2003; Ghabrial and Krasnow, 2006). As perturbations of capillary branching are associated with various pathologies, understanding the fundamental mechanisms of capillary tubulogenesis is critical to prevent or revert vascular disease. An important unresolved question is whether tip cells constitute a

homogeneous cell population, or if they require additional stage—or organ-specific signals to develop their complex branching patterns. We addressed tip cell heterogeneity by focusing on the mouse retina.

The mammalian retina is a light-sensitive tissue required for vision. The vascularization of the murine retina occurs in three distinct phases. First, new blood vessels start sprouting at post-natal day (P) 1 from the optic stalk and migrate on the retina surface toward the periphery until P7. Next, angiogenic sprouts break loose from superficial capillaries and dive into the deep outer plexiform layer, followed by the formation of the intermediate vascular plexus in the inner plexiform layer that is completed by P21 (Milde et al., 2013; Stahl et al., 2010). Vascularization of the human retina begins during late gestation and occurs in three distinct phases as well (Gariano, 2010).

Diving tip cells invade the neuroretina starting at around P6, about the same time as light-dependent photoreceptor activity becomes detectable and is followed by eye opening at P10 and full photoreceptor activation at P14 (Weiner et al., 2019; Rapaport et al., 2004; Tiriac et al., 2018). Along with the acquisition of visual function, retinal blood vessels develop a blood-retina barrier (BRB), which restricts permeability and protects neuronal functions, analogous to the function of the blood-brain barrier (BBB). The BRB is established at P10 (Chow and Gu, 2017) and is fully mature at P18 (Mazzoni et al., 2017). Hence, contrary to superficial tip cells, diving tip cells are linked to BRB maturation and neuronal activity.

Superficial retinal angiogenesis has become a reference model to characterize mechanisms regulating tip cells. Superficial (S) tip cells display a specific molecular signature, characterized by migratory properties, permeability, glycolytic metabolism, and expression of markers such as DLL4, VEGFR2, UNC5B, and ESM1 (Chow and Gu, 2017; De Bock et al., 2013; del Toro et al., 2010; Rocha et al., 2014; Strasser et al., 2010; Jakobsson et al., 2010; Geudens and Gerhardt, 2011). VEGF and NOTCH1 signaling are master regulators of S-tip cell specification (Blanco and Gerhardt, 2013). The mechanisms governing sprouting into the deep layers are not as well understood (Milde et al., 2013), even though we know that radial Müller glia expression of WNT and TGF-β ligands guides the diving sprouts (Allinson et al., 2012; Junge et al., 2009; Xu et al., 2004; Ye et al., 2009). Lack of WNT signaling prevents BRB and deeper vascular layer formation in mice and human patients with familial exudative vitreopathy (FEVR) (Gilmour, 2015), underscoring that understanding mechanisms of tip cell diving is relevant for human retinal diseases.

Here, we report that the diving D-tip cells are qualitatively different from the S-tip cells that guide superficial layer formation. D-tip cell specification depends on TGF-β signaling, and endothelial-specific loss of TGF-β receptor I (ALK5) in the post-natal retina reverts D-tip cells to an S-like phenotype, inhibiting neuroretina vascularization. Our data show that phenotypic and functional tip cell heterogeneity is required for proper post-natal retina vascularization.

RESULTS

Identification of temporal retinal EC heterogeneity

We subjected retinas from post-natal days 6 and 10 to single-cell RNA sequencing (scRNA-seq). Because endothelial cells (ECs) represent about 0.6% of retinal cell populations (Macosko et al., 2015), ECs were enriched using CD31-coated beads and magnetic cell sorting (MACS) columns (Figure 1A). Pooling 4 retinas per time point, 22,933 cells were sequenced, with an average of 42,464 reads and 1,843 genes per cell (Table S1). After filtering out low-quality cells and predicted doublets, graph-based clustering and annotation were performed based on gene expression profiles (Tables S2A and S2B), and uniform manifold approximation and projection (UMAP) plots were used for visualization. We annotated all retinal cell populations based on published markers (Macosko et al., 2015), including 1,906 ECs representing about 10% of retinal cells (Figures 1B and S1A-S1C). Subsequently, we selected *Pecam1*$^{+}$;*Cldn5*$^{+}$ EC clusters at P6 and P10 (Figure 1C), and identified venous (*Hmgn2*^{high};*Ptgis*^{high}), proliferative (*Mki67*$^{+}$;*Birc5*$^{+}$), capillary (*Mfsd2a*^{high};*Slc22a8*^{high}), arterial (*Unc5b*$^{+}$;*Bmx*$^{+}$), and tip cell EC clusters (*Kcne3*$^{+}$;*Angpt2*$^{+}$) (Figures 1D, 1E, and S1D; Tables S3A and S3B). Compared with P10 retinas, P6 retinas had more venous (13% versus 8.3%) and proliferative (44.8% versus 25.7%) ECs and less capillary (32.6% versus 41.7%), arterial (2.5% versus 7%), and tip ECs (7.2% versus 17.1%) (Figure 1F). P6 venous, proliferative, and arterial ECs clustered together with the respective P10 clusters, suggesting transcriptomic similarities between these time points. However, a comparison of the 100 most expressed genes per cluster and time point revealed significant changes in gene expression between P6 and P10, pertaining to EC maturation, arteriovenous specification, EC proliferation, and BRB establishment (Figure S1E). Moreover, we could identify two separate sub-clusters of tip ECs, both expressing previously validated tip cell markers, such as *Mcam, Chst1, Nid2*, and *Rhoc* (del Toro et al., 2010; Zhao et al., 2018) (Figure 1G). These tip cell sub-clusters were either exclusively *Esm1*$^{+}$ and mostly composed of P6 tip cells (94%) (annotated as superficial or S-tip cell cluster), or exclusively *Apod*$^{+}$ and mostly composed of P10 tip cells (88%) (annotated as diving or D-tip cell cluster) (Figures 1G, 1H, and S2A). We identified several markers to distinguish S- from D-tip cells, such as *Angpt2* and *Plvap* (high in S-tip cells), *Cldn5* and *Mfsd2a* (high in D-tip cells) (Figures 1I and S1E; Table S3C). Cell-cycle analysis revealed that both S- and D-tip cells proliferated to some extent (Figure S1F). Next, we validated these results by immunostaining. We could label S, but not D-tip cells with an antibody against ESM1, while D-tip cells but not S-tip cells expressed CLDN5 (Figures 1J and 1K). Moreover, we performed lineage tracing of retinal tip cells using *Mfsd2aCreER*^{T2};*mTmG* reporter mice. Tamoxifen (TAM) administration activated green fluorescent protein (GFP) expression in CRE-expressing cells and revealed that *Mfsd2aCreER*^{T2}-mediated recombination labeled D-tip cells, but not S-tip cells (Figures 1J and 1K). Taken together, our results show that two distinct tip cell populations exist during superficial and deep layer vessel formation in the post-natal retina.

Identification of specialized neuroretina D-tip cell

To characterize signaling pathways in different EC clusters, we performed gene set variation analysis (GSVA) with in-house-generated gene sets, compiled from the GSEA database

(Tables S4A and S4B). Arterial, venous, and capillary ECs highly expressed genes involved in BRB and WNT signaling, such as *Cldn5, Spock2, Lef1*, and *Adgra2* (Figures 2A and 2B). S-tip cells had the lowest score in these pathways, while D-tip cells showed increased expression of BRB- and WNT-related genes, consistent with BRB establishment around P10 (Figures 2A, 2B, and S2B). Several studies have shown that differential activation of metabolic pathways controls angiogenesis (De Bock et al., 2013; Dumas et al., 2020; Schoors et al., 2015). GSVA analysis showed that proliferative ECs have the highest TCA-cycle score, while S-tip cells have the highest glycolysis score. On the other hand, D-tip cells have lower TCA-cycle and glycolysis scores than S-tip cells (Figures 2C and S2C). Gene-level analysis of TCA-cycle genes and glycolytic sets showed lower expression of *Eno1, Pgm1, Dlst*, and *Mdh2* in D-tip cells compared with S-tip cells (Figure 2D). Moreover, ECs produce extracellular matrix (ECM) proteins to form the basement membrane of the new vessels. D-tip cells exhibited higher ECM gene and ECM gene regulator GSVA scores than S-tip cells did, including *Sparc* and *Serpine1* (Figures 2E, S2D, and S2E). Overall, the data show that D-tip cells differ from S-tip cells in BRB properties, metabolic requirements, and the ECM.

TGF-β signaling is suppressed in superficial S-tip cells (Aspalter et al., 2015), prompting us to run GSVA of TGF-β pathway activation using in-house generated gene sets. Interestingly, we observed higher TGF-β signaling scores in D-tip cells compared with all other EC clusters (Figure 2F; Table S4B). In particular, D-tip cells showed enriched expression of TGF-β target genes, such as *Pmepa1, Cdh2, Fn1, Cdkn1a*, and *Cdh11* (Figure 2G). Analysis of TGF-β ligand expression in all retinal clusters revealed that *Tgfβ1* was mainly expressed by immune cells, *Tgfβ2* by astrocytes, bipolar cells, and Müller glial cells, and *Tgfβ3* by Müller glial cells and pericytes (Figures 2H and S2F). *Tgfβ2* and *Tgfβ3* expression was increased by Müller glial cells between P6 and P10 (Figure 2H). Our data also confirmed that Müller glia was the principal source of *Vegfa* at P10, and *Vegfa* expression was two times lower than *Tgfβ2* at P10 (Figures S2F and S2G). ECs expressed both *Tgfβ receptor 2* (Tgfβr2) and *Tgfβr1* (*Alk5*), but *Alk5* expression was sharply increased in D-tip cells, suggesting a signaling requirement in D- versus S-tip cells (Figure 2I).

Endothelial TGF-β signaling is essential for neuroretina vascularization

To examine the function of ALK5 in ECs, we generated inducible, endothelial-specific *Alk5* mutants (*Alk5iEKO*) by crossbreeding *Alk5* conditional mice (Larsson et al., 2001) with *Cdh5CreER*^{T2} (Wang et al., 2010) mice (Figure 3A). TAM-injected Cre-negative *Alk5*$^{fl/fl}$ littermates were used as controls. Following TAM administration, *Alk5* deletion was confirmed by qRT-PCR using mouse brain ECs isolated from *Alk5*$^{fl/fl}$ and *Alk5iEKO* mice (Figure 3B). TGF-β-induced SMAD2/3 phosphorylation was abolished in *Alk5iEKO* cells, attesting efficient gene deletion (Figure 3C). *Alk5* deletion between P0 and P3 did not affect retinal vascular outgrowth but reduced the vascular area and produced fewer and wider angiogenic sprouts when compared with controls (Figures 3D and 3E). At P12, *Alk5iEKO* retinas displayed striking vascular malformations. Instead of forming the deep vascular layers, glomeruloid neovascular tufts (NVTs) developed throughout the retina vasculature (Figures 3F and 3G). Cross-sections of mouse eyes showed that the *Alk5iEKO* retinas completely lacked the deep vascular layer and that the descending sprouts did not extend

beyond the inner nuclear layer (Figure 3H). TAM administration between P6 and P8, when deep vascular plexus formation is initiated, phenocopied early post-natal deletion (Figures S3A and S3B). Time course analysis of vertical sprouting between P9 and P11 showed that *Alk5* deficient ECs were able to initiate vertical sprouting but failed to progress into the deeper layers (Figures S3C-S3E). The vascular malformations did not resolve with age, and at P21, *Alk5iEKO* retinas looked very similar to their P12 counterparts (Figures S3F and S3G). Moreover, global deletion of *Alk5* using the *R26CreER*^{T2} line, phenocopied the vascular defects of the *Alk5iEKO* retinas at P12, suggesting that TGF-β signals primarily in ECs to drive neuroretina vascularization (Figures S3H and S3I).

TGF-β signaling is required for D-tip cell differentiation

To investigate how TGF-β signaling controls neuroretina vascularization, we used scRNA-seq to compare the transcriptomic profiles of *Alk5iEKO* versus littermate control retinas at P10. We sequenced 35,728 cells from 4 retinas per condition, with an average of 36,620 reads per cell, and 1,656 genes per cell (Table S1). Retinal cells were clustered and annotated using known marker genes (Figures S4A-S4D; Tables S2A and S2B). Following graph-based sub-clustering of *Pecam1*$^{+}$;*Cdh5*$^{+}$ ECs, we annotated the EC sub-clusters as venous, proliferative, capillary, arterial, and tip cell EC clusters (Figures 4A and S4E). To overcome batch effects, we used the Seurat V3 SCTransform-Integration method to combine control and *Alk5iEKO* P10 EC data (Figure S4F). *Alk5* deletion significantly increased the number of proliferating ECs and decreased the number of tip cells (Figures 4B and S4G). We confirmed that TGF-β signaling decreased in *Alk5iEKO* compared with control ECs, using GSVA and two TGF-β target gene sets (downregulated or upregulated by TGF-β) (Figures 4C, S4H, and S4I; Tables S5A and S5B). Gene expression analysis in the tip EC cluster showed that *Alk5* deletion induced loss of D-tip cell identity, while promoting an S-tip-cell-like identity (Figures 4D and 4E; Table S5C). Indeed, the expression of D-tip cell markers (e.g., *Apod* and *Pmepa1*) decreased, while the expression of S-tip cell markers increased (e.g., *Esm1* and *Plvap*) in *Alk5iEKO* tip cells (Figures 4F and S4J; Table S5A). BRB- and WNT signaling-related genes were decreased in *Alk5iEKO* tip ECs (Figures 4G and 4H; Table S5A). While loss of TGF-β signaling in ECs increased expression of genes related to the TCA cycle (e.g., *Fh1* and *Pdha1*), it decreased glycolysis and ECM gene expression (e.g., *Pfkfb3, Lamb1*, and *Ctsw*) (Figures 4I, 4J, and S4K; Table S5A). *In vivo, Alk5iEKO* retinas showed ectopic expression of the S-tip cell marker ESM1, while expression of the D-tip cell marker CLDN5 was significantly reduced at P12, confirming the inability of ALK5-deficient ECs to acquire the D-tip cell identity (Figure 4K). Finally, we looked at the effects of *Alk5* loss of function in the acquisition of S-tip cell identity at P6 by scRNA-seq (Figures S4L-S4U). The number of S-tip cells was not affected by *Alk5* deletion (4.5%, Figure S4R). Although the expression of genes such as *Esm1* and *Plvap* remained unchanged in *Alk5iEKO* S-tip cells (Figure S4S), the overall transcriptomic profile of S-tip cells was altered in the *Alk5iEKOs* (Figures S4T-S4U; Table S5D), suggesting some involvement of TGF-β signaling in S-tip cell transcriptional identity.

Inhibiting proliferation or WNT overactivation does not rescue *Alk5iEKOs*

Since the cluster of proliferating ECs was increased in the *Alk5iEKOs*, we analyzed EdU incorporation in P12 *Alk5iEKO* retinas. The mutant ECs proliferated more than

their littermate controls in capillaries and veins, but not in arteries (Figures 5A and 5B). We treated mutant and control littermate pups with Palbociclib, an inhibitor of the cyclin-dependent CDK4 and CDK6 kinases (Finn et al., 2009) (Figure 5C). Daily administration of Palbociclib between P7 and P12 reduced the vascularization of the deep layer in the controls and decreased the number of proliferating (EdU+) ECs in the mutant NVTs (Figures 5D and 5E); yet, it did not improve deep layer vascularization in the mutants (Figures 5F and 5G). We confirmed these results by treating pups with mitomycin C, a potent cell-cycle inhibitor. One single dose of mitomycin C at P7 dramatically decreased the amount of EdU+ ECs in NVTs but failed to rescue deeper layer formation in the mutants (Figures S5A-S5E), suggesting that increased EC proliferation is not causing the decreased deeper retina vascularization in the *Alk5iEKOs*.

WNT signaling is important for intraretinal capillary plexus formation and *Alk5iEKOs* showed decreased expression of WNT-signaling-related genes at P10 (Figures 4G and 4H). To investigate whether reduced WNT signaling is responsible for the vascular defects observed in the *Alk5iEKO* retinas, we crossbred *Alk5iEKO* mice with mice expressing a stable beta-catenin in ECs (β-*Catenin*$^{flox(ex3)}$) (Harada et al., 1999). Activation of WNT signaling did not affect deep layer vascularization in the *Alk5iEKOs* (Figures 5H and 5I), but reduced the macroscopic retinal hemorrhage observed in the mutants (Figure 5J). In addition, WNT activation decreased the expression of plasmalemma vesicle-associated protein (PLVAP) and increased the expression of CLDN5 in *Alk5iEKO* mice (Figures 5K, 5L, and S5F).

Targeting hypercontractility improves vascularization in *Alk5iEKO* retinas

Endothelial TGF-β signaling is important for EC-pericyte interactions (Allinson et al., 2012; Armuliket al., 2011), and pericytes are essential for deep vascular plexus and BRB formation (Park et al., 2017). We therefore investigated whether endothelial *Alk5* deletion affected pericyte function. We found increased expression of *Acta2* and myofibroblast markers, such as *Vim* and *Tagln* as well as *Rock2*, in *Alk5iEKO* pericytes, but not ECs (Figure 6A). In addition, loss of *Alk5* decreased the EC expression of BRB genes that are controlled by pericytes (Mäe et al., 2021) (Figure S6A). Lineage tracing analysis using *Cdh5CreER*^{T2};*Alk5*$^{lox/lox}$;*mTmG* mice did not show α-SMA^{+};GFP^{+} ECs in the retinal tufts, suggesting absence of endothelial to mesenchymal transition but abnormal pericyte differentiation in *Alk5iEKO* retinas (Figure 6B). *Alk5iEKO* retinas showed excessive immunoreactivity for α-SMA (Figure 6C), which is encoded by *Acta2* and is expressed by dysfunctional retinal pericytes (Dubrac et al., 2018). Increased α-SMA expression and stress fiber contractility depend on ROCK activity and myosin light chain (MLC2) phosphorylation on Thr18 and Ser19. We detected increased pMLC2 immunostaining in the *Alk5iEKO* compared with control retinas (Figure 6C), which overlapped with increased α-SMA expression (arrowheads in 6c), while blood vessels devoid of α-SMA coverage were pMLC2 negative (arrows in 6c). GSVA analysis for RhoA-GTPase pathways showed reduced Rho-GTPase scores in D-tip cells in *Alk5iEKOs* versus controls, while *Rock2* increased in *Alk5* mutant pericytes (Figures 6A and S6B; Table S5E), suggesting that ROCK inhibition could rescue *Alk5iEKO* retinas. Treatment with Fasudil, a potent ROCK inhibitor, could significantly reduce pMLC2 immunoreactivity and α-SMA expression in the mutant

retinas (Figures 6D–6F and S6C). Daily treatment of the mice with Fasudil between P6 and P11 improved vascularization of the deep layer in the *Alk5iEKOs* and decreased the number of NVTs (Figures 6G, 6H, S6D, and S6E).

Non-canonical TGF-β signaling promotes D-tip cell sprouting

Binding of TGF-β to ALK5 activates SMAD2 and SMAD3, which complex with SMAD4 to regulate the expression of TGF-β-target genes (Shi and Massague, 2003). To test if SMAD2/3 signaling was involved in the formation of the deep retinal plexus, we generated endothelial SMAD2 and SMAD3 mutants by crossing *Cdh5CreER^{T2}* mice with mice carrying floxed alleles of *Smad2* (Ju et al., 2006) and *Smad3* (Li et al., 2008) (*Smad2/3iEKO*). TAM administration between P0 and P3 revealed a similar phenotype to the *Alk5iEKO* retinas at P6, characterized by reduced vascular area and fewer sprouts, and a slightly reduced radial migration (Figures S7A-S7C). Ectopic expression of α-SMA could be seen on the angiogenic sprouts of the *Smad2/3iEKOs* (arrowheads in Figure S7B). Analysis of the mice at P12 showed that the mutant retinas exhibited a hypovascular phenotype, featuring reduced radial migration, fewer descending sprouts, and a slight decrease in deep layer vascular density (Figures 7A-7E). However, we did not observe any NVTs, and the phenotype resolved by P21 (Figures S7D-S7F). Single-mutant mice for *Smad2* or *Smad3* resulted in a similar, although less severe phenotype compared with the compound mutants (Figures S7G-S7R). These results indicate that SMAD2 and SMAD3 are proangiogenic during primary and secondary plexus formation in the retina, and their function is partially redundant. To corroborate these results, we analyzed endothelial-specific mutants for the common SMAD4 (*Smad4iEKO*) (Yang et al., 2002). The *Smad4iEKOs* partially recapitulated the *Smad2/3iEKOs* at P12, exhibiting a reduction in the number of vertical sprouts and deep layer density, as well as increased α-SMA immunoreactivity (Figures 7F-7H). Like *Smad2/3iEKOs*, the SMAD4-deficient ECs did not form NVTs, although they displayed arteriovenous malformations (yellow arrows in Figure 7G), as reported before for EC-specific *Alk1* and *Smad4* mutants (Ola et al., 2018,2016; Tual-Chalot et al., 2014; Crist et al., 2018). In addition, immunofluorescent staining for various targets that were significantly altered in the *Alk5iEKO* retinas, showed no changes in the *Smad2/3iEKOs* at P12, including APOE, TXNRD1, PLVAP, and VWF (Figure 7I), confirming SMAD-independent regulation of those genes by TGF-β.

TGF-β is essential for retina revascularization in OIR

In ischemic retinopathies such as proliferative diabetic retinopathy (PDR) and retinopathy of prematurity (ROP), VEGF induces tip cell specification and sprouting to revascularize the retinal tissue (Sapieha et al., 2010). However, some tip cells fail to form proper vessels and develop pathological NVTs that are leaky and prone to bleeding. To study the contribution of TGF-β signaling to ocular neovascular disease, we used the OIR mouse model, which mimics some aspects of the vascular defects of human ROP and PDR. Hyperoxia (75% O_2) exposure of neonatal mice between P7 and P12 triggers vaso-obliteration. Hypoxic neurons then secrete excessive amounts of VEGF, which leads to pathological sprouting and formation of NVTs from P12-P17 (Figure S8A) (Sapieha et al., 2010). We analyzed previously published scRNA-seq data of normoxia and OIR retinas (Binet et al., 2020). Compared with normoxia, both *Vegf* and *Tgfβ2* expression were strongly increased in P17

OIR Müller glia cells (Figures 8A and S8B-S8E; Table S6A). In contrast to healthy P10 retinas, we found approximately three times more *Vegf* than *Tgfβ2* expression in the OIR retinas (Figure S8F). Because of the low EC numbers in these scRNA-seq samples, we sub-clustered and integrated the *Pecam1*$^{+}$;*Cdh5*$^{+}$ ECs from P17 normoxia and OIR with our own P6 and P10 EC datasets to improve tip cell identification (Figures S8G and S8H). After bioinformatics isolation of tip cells using well-known markers, such as *Clec1a* and *Chst1*, P17 normoxia and OIR tip cells were compared with S- and D-tip cells (Figures S8I and S8J; Table S6B). While we could identify D-tip cells in the P17 normoxia retinal ECs, tip cells in the OIR retinal EC were more S-like. OIR tip cells expressed a high level of *Esm1* and were negative for *Mfsd2a*, while they expressed higher levels of TGF-β target genes and *Alk5* (Figures 8B-8D). We confirmed this finding in *Mfsd2aCreER*^{T2}*;mTmG* mice, exposed to OIR. At P17, 24 h after TAM injection, all tip cells were ESM1 positive and GFP (MFSD2A) negative, confirming S-like tip cell identity (Figure 8E). To determine whether TGFβ/ALK5 signaling contributes to retinal revascularization or NVT formation, we subjected *Alk5iEKO* mice to OIR (Figure 8F). At P17, *Alk5iEKO* mice showed increased NVT formation and reduced revascularization (Figures 8G-8I). In fact, all revascularizing sprouts formed NVTs (arrows in Figure 8H) with increased α-SMA+ pericyte coverage in the *Alk5iEKOs* compared with control retinas.

DISCUSSION

EC heterogeneity has been demonstrated across different adult organs and tissues, highlighting the plurality of EC phenotypes that represents an enormous untapped therapeutic potential (Augustin and Koh, 2017; Potente and Makinen, 2017). Here, we show that molecular heterogeneity also characterizes angiogenic tip cells, by identifying a new tip cell type that controls vascularization of the neuroretina deep layers (Figure 8J). Diving tip cells originate from capillaries and veins and a few D-tip cells can be identified as early as P6. These nascent D-tip cells already have a distinct molecular identity compared with S-tip cells (Figures S2B-S2D), suggesting that they are a unique population that do not originate from S-tip cells. Contrary to S-tip cells, D-tip cells have increased barrier properties. The BRB controls para- and transcellular EC permeability and depends on tight junction proteins, such as CLDN5, which is mainly controlled by WNT signaling (Wang et al., 2020), as well as on pericytes that regulate the expression of the lipid transporter MFSD2A (Chow and Gu, 2017; Andreone et al., 2017; Armulik et al., 2010; Ben-Zvi et al., 2014). D-tip cells upregulate both CLDN5 and MFSD2A expression and have a stronger WNT and BRB transcriptomic and molecular signature than S-tip cells, confirming that D-tip cell sprouting and initiation of BRB formation are functionally coupled.

WNT signaling is also essential for deep layer formation in the retina (Chen et al., 2012; Ye et al., 2009; Xu et al., 2004; Xia et al., 2008; Luhmann et al., 2005). While our data suggest crosstalk between ALK5 and WNT signaling, activation of WNT signaling through genetic overexpression of β-catenin in ECs improved the junctional defects and hemorrhage but did not rescue the vascular malformations in *Alk5iEKO* retinas. Whether β-catenin gain of function improves vascular leakage in the *Alk5iEKOs* remains to be determined.

D-tip cell identity is likely regulated by TGF-β2, expressed mainly by Müller glia. We found increased retinal expression of *Tgfβ2* between P12 and P17, while *Alk5* expression peaks between P10 and P15 in retinal ECs (Jeong et al., 2017), suggesting a requirement for TGFβ/ALK5 signaling for D-tip cell specification during that time. In line with this, diving *Alk5iEKO* tip cells failed to acquire the D-tip cell identity, leading to EC migration defects and aberrant EC proliferation. Surprisingly, canonical TGF-β signaling was found to be dispensable for D-tip cell specification. Although *Smad2/3* and *Smad4* endothelial-specific mutant mice displayed a transient delay in deep layer vascularization, neither mutant phenocopied the *Alk5iEKOs*, nor did they exhibit the gene expression changes seen in the *Alk5iEKOs*, providing genetic evidence that deep layer formation primarily requires non-canonical ALK5 signaling. Such non-SMAD mediated signaling includes MAP kinase, RHO-GTPase, and phosphatidylinositol-3-kinase/AKT pathways, regulating epithelial to mesenchymal transition, cell proliferation, and migration (Chen et al., 2019; Massagué, 2012; Akhurst and Hata, 2012; Zhang, 2017). How these non-canonical signaling pathways regulate D-tip cell identity during neuroretina vascularization requires further investigation.

Our next main finding is that endothelial ALK5 signaling maintains pericyte function. Pericyte depletion in the postnatal retina induces BRB breakdown, sprouting defects, lack of deep vascular plexus formation, and increased ESM1 expression in S-tip cells (Dubrac et al., 2018; Eilken et al., 2017; Park et al., 2017). A recent scRNA-seq analysis of brain EC from mice lacking pericytes (*PDGFRβ*$^{ret/ret}$ mice) has identified endothelial BBB genes controlled directly by pericytes, such as *Mfsd2a, Tfrc*, and *Slc16a1* (Mäe et al., 2021). Endothelial *Alk5* deletion decreased the expression of those genes in ECs, indicating defective EC-pericyte interactions in the mutant retinas. *Alk5iEKO* retinas are covered with abnormal pMLC2-expressing pericytes. Cell contractibility is mainly regulated by the serine/threonine kinases ROCK1/2, which phosphorylate MLC to promote stress fiber assembly (Amano et al., 1996; Kureishi et al., 1997; Totsukawa et al., 2000). Fasudil treatment decreased pMLC2 staining and improved neuroretina vascularization in the *Alk5iEKOs*, suggesting that pericyte dysfunction in the mutant retinas contributes to vascular malformations. Yet, since Fasudil does not specifically target mural cells, effects on other cell types, such as ECs and Müller glia cells, cannot be excluded. In addition, the exact mechanisms leading to pericyte dysfunction and the consequences of pericyte differentiation in retina vascularization require further studies.

Finally, we show that TGF-β signaling is essential for retina revascularization in OIR. We observed formation of abnormal S-like tip cells in the P17 OIR retina that expressed high levels of ALK5 and increased TGF-β signaling compared with normal P6 S-tip cells. Genetic deletion of *Alk5* suppressed retina revascularization and exacerbated the vascular lesions during OIR. Altogether, our findings show that TGF-β signaling in tip cells promotes retina revascularization and prevents NVT formation in OIR (Figure S8K), suggesting that TGFβ/ALK5 activation could provide an alternative therapeutic approach for the treatment of retinopathies (Miller et al., 2013).

Tip cells are indispensable components of sprouting angiogenesis in all organs of large multicellular organisms during development and disease. Further exploration and identification of the mechanisms controlling tip cell heterogeneity will allow more tailored

approaches to prevent excessive neovascularization in ischemic diseases in the retina and other prevalent diseases such as cancer, stroke, and coronary artery disease.

Limitations of the study

The signaling function of SMAD2/SMAD3 in retinal angiogenesis remains to be determined. Both *Alk5iEKO* and *Smad2/3iEKO* mutants showed defective retinal vascularization at P6, indicating that canonical ALK5 signaling is involved in the formation of the superficial vascular plexus. *Tgfβ1*$^{-/-}$ mutants lack the deep retinal vascular plexus (Arnold et al., 2012), as do mice lacking integrin αvβ8, which is required for TGF-β activation (Hirota et al., 2011). These phenotypes have been attributed to reduced SMAD2/SMAD3 signaling in ECs; yet, these mice do not fully phenocopy the *Alk5iEKO* mice. The *Tgfβ1*$^{-/-}$ mutants can still form the intermediate vascular plexus, whereas the *Tgfβr2iEKO* (Allinson et al., 2012) and *Alk5iEKO* (Figure 4) are unable to dive into the neuroretina. This suggests that ligands other than TGF-β1 (such as TGF-β2) could also activate non-canonical ALK5 signaling to mediate deep layer vascularization. Moreover, the upstream molecular regulators determining *Alk5* expression in ECs during this time window remain to be determined.

STAR★METHODS

RESOURCE AVAILABILITY

Lead contact—Requests for reagents and data should be directed to and will be fulfilled by the lead contact, Alexandre Dubrac (alexandre.dubrac@umontreal.ca).

Materials availability—Materials are available upon reasonable request.

Data and code availability—All data that support the findings of this study are available within the article and its supplemental information File and from the corresponding author upon reasonable request. The scRNAseq data discussed herein will be deposited in NCBI's Gene Expression Omnibus (accession no. GSE175895).

EXPERIMENTAL MODEL AND SUBJECT DETAILS

Mice—All mouse experiments were reviewed and approved by the Yale University Institutional Animal Care and Use Committee (IACUC) and the ethical committee of the CHU Sainte-Justine Research Centre. *Alk5*^{flox}, *Smad2*^{flox}, *Smad3*^{flox} (kindly provided by M. Matzuk), *Smad4*^{flox}, *β-Catenin*$^{flox(ex3)}$ and *mT/mG* reporter mice (Muzumdar et al., 2007) were crossed with *Cdh5CreER*^{T2} mice (kindly provided by R. Adams), *R26CreER*^{T2} (Ventura et al., 2007), or *Mfsd2aCreER*^{T2} (Pu et al., 2018) mice. To induce postnatal gene deletion, mice were injected intragastrically with 100μg of tamoxifen (TAM) (Sigma, T5648; 25 mg/ml in corn oil) for three consecutive days and analyzed as indicated. TAM-treated, Cre-negative littermates were used as controls. For lineage tracing studies using the *Mfsd2aCreER*^{T2} line the mice received 100μg of TAM 24 h prior to sacrifice. The ROCK inhibitor Fasudil-Hydrochloride (CDS021620, Sigma) was dissolved in sterile PBS and injected intraperitoneally (20ug/g). The cell-cycle inhibitors Palbociclib (PD 0332991 isethionate, PZ0199, Sigma) was dissolved in NaLactate and administered intragastrically

daily (50μg/g), while Mitomycin C (AC226940020, Fisher Scientific) was dissolved in sterile H_2O and administered intraperitoneally once at P7 (20ul/g).

Oxygen-induced retinopathy—Retinal angiogenesis was induced by placing P7 pups with their nursing mothers in a hyperoxia chamber with a calibrated controller and an oxygen sensor (BioSpherix) and exposing them to 75% O_2 until postnatal day P12. Mice were then placed in room air until P17. For the OIR experiments in *Alk5iEKO* mice, the pups were induced with TAM between P5-P7.

Single cell RNA sequencing

Tissue dissociation and sample preparation: 4 retinas from P6 or P10 pups were dissected and dissociated with a modified version of the Neural Tissue Dissociation kit (P) (Miltenyi Biotec, Cat#130- 092-628). The retinas were digested 5min in buffer P supplemented with DNase I (2000U/mL, Qiagen #79254). The digestion was stopped by adding FBS (10% final) and the cells were immediately filtered through a 70μm cell strainer. After centrifugation (300g for 3min), the cells were resuspended in PBS supplemented with 2mM EDTA and 0.5% BSA. The single cell suspension was enriched for ECs using CD31 MicroBeads (Miltenyi Biotec, Cat#130-097-418) according to the manufacturer's instructions.

Library preparation and sequencing: Single cell suspensions of retinal cells were resuspended in PBS containing 0.04% ultra-pure BSA. scRNAseq libraries were prepared using the Chromium Single Cell 3′ Reagent Kits v3.1 (10x Genomics; Pleasanton, CA, USA) according to the manufacturer's instructions. The target cell recovery for each library was 10,000. Generated libraries were sequenced on an Illumina HiSeq4000, followed by de-multiplexing and mapping to the mouse genome (mm10-3.0.0) using CellRanger (pipeline version 3.1.0) (10x Genomics).

Data processing and EC clustering: Gene expression matrices were generated using CellRanger (10x Genomics). Further processing and analysis of the data were performed using R (version 3.6.0). For each EC MACS-enriched sample, the raw unfiltered gene expression matrix was analyzed for empty droplets containing ambient RNA using the *emptydrops* function from the DropletUtils R-package (version 1.6.1) (Lun et al., 2019). The raw data were also analyzed for cell doublets using Solo (version 0.5, running in Python 3.8.2) (Bernstein et al., 2020), a semi-supervised deep learning doublet detection tool. Barcodes identified as empty droplets or cell doublets were filtered out. Further analysis was performed using tools from the Seurat R-package (version 3.2.2) (Stuart et al., 2019). Additional quality control steps filtered out genes that were expressed in less than 10 cells and cells that expressed fewer than 100 genes. Lastly, only cells which had fewer than 60000 counts, between 500 and 7500 genes and less than 10% of the unique molecular identifiers (UMIs) originating from mitochondrial genes were retained for further analysis. Normalized gene expression data, generated using the *NormalizeData* function, was used for differential gene expression analysis. We could not observe any decrease in the mRNA level of *Tgfbr1* in the ECs isolated from *Alk5iEKO* retinas. This is because the 10X genomics kit captures the polyA mRNA and generates libraries from

the 3′ UTR, suggesting that the exon deletion does not decrease the total mRNA level, but nevertheless generates a loss-of-function *Alk5* mutation, as evident from Figures 3A-3C. For visualization, individual samples were normalized using the *SCTransform* function. Seurat v3-SCTransform multiple dataset integration was performed on merged P6-P10 Control and P10 Control-*Alk5iEKO* datasets to correct for batch effects. Dimensional reduction of the data were performed using Uniform Manifold Approximation and Projection (UMAP) (arXiv:1802.03426) as implemented in the *RunUMAP* function, where the number of PCA dimensions used for the *dims* parameter was adjusted on a per-dataset basis and all other settings were default. Louvain graph-based clustering was performed on a shared nearest neighbor graph, generated using the first two UMAP dimensions as input. Extensive over-clustering and careful analysis of gene expression in each cluster was conducted to account for possible artifacts arising from UMAP-based clustering. Cell clusters were annotated based on well-known marker gene expression, namely, EC clusters were identified by the presence of *Cldn5* and *Pecam1* expression. ECs, separately identified from the P6 and P10 Control samples, were merged, but not integrated. The first 10 PCs were used to run UMAP and metadata regression on the batch and percent of mitochondrial genes was performed during SCTransformnormalization. P10 Control replicate, D7, contained relatively few ECs and produced a significant batch effect. It was therefore not included in the analysis of the P6-P10 Control EC data. P10 ECs, separately identified from Control and *Alk5iEKO* samples, were integrated due to noticeable batch effects. The first 15 PCs were used to run UMAP and metadata regression on nCount_RNA, nFeature_RNA and the percent of mitochondrial genes was performed during SCTransform normalization, prior to integration. Whenever possible, it was preferred to not use anchor-based dataset integration methods so as to avoid oversmoothing. UMAP and graph-based clustering were repeated on the subclustered EC datasets, as previously described.

Gene set analyses—The normalized gene-by-cell expression matrices were converted into gene-set-by-cell matrices using Gene Set Variation Analysis (GSVA) (Hänzelmann et al., 2013), and a collection of expert annotated gene sets generated in-house using information from the Molecular Signatures Database (MSigDB; version 7.2) (Liberzon et al., 2015, 2011; Subramanian et al., 2005). Gene sets were formatted for GSVA as a *GeneSetCollection* object using the GSEABase R-package (version 1.48.0) (Morgan et al., 2021). GSEABase: Gene set enrichment data structures and methods. R package version 1.52.0.) and GSVA was performed using default parameters as implemented in the GSVA R-package (version 1.34.0). The adj pvalues for all GSVAs shown in the manuscript are provided in the Tables S4A, S5A, and S5E.

Analysis of publicly available EC data—We used the publicly available processed scRNA-seq data and metadata for P17 normoxia and OIR retinas (Binet et al., 2020). The raw data were extracted from NCBI's Gene Expression Omnibus (accession no. GSE150703) and further processed as described above. Due to the low number of ECs in this dataset, we integrated the P17 OIR-Normoxia ECs with the P6-P10 Control ECs from this study. ECs from the P17 OIR-Normoxia dataset that clustered with tip cells from the P6-P10 Control dataset were labelled as tip cells.

In situ hybridization (ISH)—RNAscope ISH (AdvancedCell Diagnostics, Biotechne) protocol was modified for whole mount OIR retina staining. Retinas were fixed in 4% PFA for 1h at RT, incubated 10min in H_2O_2, followed by 15min in protease IV (diluted 1:50 in PBS). Samples were hybridized with RNA target probes (*Tgfβr1*, nt 2257-3252 of NM_009370.2, Channel 1; #406201) overnight at 40°C. After amplification and probe labeling, the retinas were further stained with IsoB4.

Primary brain endothelial cell (mBEC) isolation and *Alk5* inactivation—P12 pups were euthanized, and their brains were removed, placed into ice-cold buffer A (10mM *N*-2-hydroxyethylpiperazine-*N*′-2-ethanesulfonic acid, 1 × penicillin-streptomycin, 0.5% bovine serum albumin in Dulbecco's modified Eagle medium), and processed as previously described (Hale et al., 2020). Meninges and choroid plexus were removed, and brain tissue was minced with scissors. Tissue suspensions were centrifuged at 700*g* for 5min at 4°C, and the brain tissue pellet was digested with collagenase and dispase solution (DMEM containing 1mg/ml collagenase/dispase [10269638001; Sigma-Aldrich], 20units/ml DNase I [11284932001; Sigma-Aldrich], and 0.147μm/ml tosyl-lysine-chloromethyl-ketone [T7254; Sigma-Aldrich]) at 37°C for 1h. After incubation, the brain tissue was homogenized using Pasteur pipettes, and clarified by passage through a 70μm mesh filter. After centrifugation (700*g* for 5min at 4°C), the pellet was resuspended in ice-cold buffer B (10mM Hepes, 1 × penicillin streptomycin, and 25% BSA in DMEM). The suspension was centrifuged at 1000*g* for 20min at 4°C. BMECs from two brains were pooled and seeded onto 35mm collagen-coated plates and cultured in EGM-2 medium (Lonza). BMECs were cultured for 48h in 10μg/ml puromycin and maintained in 2μg/ml puromycin for 6 days. For genetic inactivation of *Alk5*, BMECs were treated for 24 h with 5μM 4-hydroxy-tamoxifen (Sigma-Aldrich; product number H7904). Thereafter, the medium was replaced with medium lacking 4-hydroxy-tamoxifen. 48h after gene deletion, BMECs were starved overnight using EBM2 media (Lonza) containing 0.5% FBS and treated for 30min with 2.5ng/ml of TGFβ1 (#8915, Cell signaling).

Quantitative real-time PCR—Total RNA was purified from mBECs using RNeasy Plus Mini Kit (Qiagen, #74134), and reverse transcribed to cDNA using iScript cDNA Synthesis Kit (Bio-Rad, #170–8891). QRT-PCR was performed using SYBR Green Supermix (Bio-rad, #1798880) and the mouse *Alk5* primers (Forward: CGCCCTTTCATTTCAGAGGG; reverse: CAATTGTTCTTTGAACAAGC). The data were first normalized to the housekeeping gene *Actb1* (Qiagen, QT00095242) for each sample, and the relative expression levels of different genes *vs.* the control samples were calculated using the comparative CT method.

Western blot—For assessment of protein levels in mouse tissues, brains were dissected, and snap frozen in liquid nitrogen. To purify primary lung ECs mouse lungs were dissected, minced, and digested in type I collagenase (Worthington Biochem. Corp., LS004196; 1mg/ml) in serum-free DMEM medium (Lonza, #12-709F) for 1h at 37°C. The tissue digest was then filtered through a 70μm cell strainer, followed by incubation with CD31 antibody-coated Dynabeads. ECs were then isolated on a magnetic separator. Purified ECs were cultured in DMEM supplemented with 10% fetal bovine serum, 1xpenicillin/

streptomycin, 100mg/ml EC mitogen (Biomedical Technologies, BT-203), and 10U heparin (Sigma, H3149) for 5-7 days, followed by a secondary sorting with ICAM-2 antibody-coated Dyna-beads. Cells were lysed in RIPA buffer (50mM Tris, pH7.4, 150mM NaCl, 1% NP-40, 0.5% sodium deoxycholate and 0.1% SDS) containing protease and phosphatase inhibitor cocktails (Roche, 11697498001 and 04906837001). Protein concentrations were measured by a BCA protein assay kit (Pierce, #23225). Equal amounts of proteins were separated on 4–15% SDS-PAGE gels (Bio-Rad, 5671084), followed by immunoblotting. Proteins were detected using the following antibodies: p-SMAD2/3 (8828, Cell Signaling 1:1000), SMAD2 (5339, Cell Signaling 1:1000), SMAD3 (9523 Cell Signaling 1:1000) and β-actin (A1978, Sigma). The blots were then probed with horseradish peroxidase–labeled secondary antibodies (Vector Laboratories), and the signal was visualized with the appropriate chemiluminescent HRP substrate (WBKLS0500, Millipore).

Immunostaining—For retina stainings, the mice were euthanized, and their eyes were collected and fixed in 4% formaldehyde for 15min at RT. After a PBS wash, the retinas were dissected and fixed in iced-cold methanol at −20°C overnight. The next day the retinas were re-fixed in 4% formaldehyde for 15min at RT, washed in PBS and processed for whole mount staining. For visualization of D-tip cells following whole-mount staining, P8-9 retinas were embedded in 3% agarose and cut into 150μm thick sections using a vibratome. For staining of sections, whole eyes were fixed in 4% formaldehyde at 4°C overnight, washed in PBS and incubated with 20% sucrose in PBS, before being immersed in OCT medium (TissueTek). For immunostaining, blocking and permeabilization was performed using blocking buffer (BB) consisting of 1% FBS, 3% BSA, 0.5% triton X100, 0.01% Na deoxycholate, 0,02 %Na Azide in PBS for 1h at RT on a rocking platform. Primary and secondary antibodies were incubated at the appropriate dilutions in BB at 4°C overnight in a rocking platform and the retinas were mounted in fluorescent mounting medium (Dako, Carpinteria, CA, USA), or Vectashield containing DAPI (Vector Laboratories). The retina vasculature was visualized using Alexa conjugated Isolectin GS-IB4 from Griffonia simplicifolia, (I21411, Invitrogen). The following primary antibodies were used: mouse anti-α-smooth muscle actin-CY3 (C6198, Sigma;1:300), goat anti-mouse PECAM1 (AF3628, R&D, 1:100), rabbit anti-GFP (G10362, Invitrogen 1:200), rat anti mouse MECA-32 (PLVAP; 553849, BD Pharmingen; 1:200), rabbit anti-mouse CLDN5 (34-1600, Invitrogen; 1:200), goat anti-mouse DLL4 (AF1389, R&D Systems; 1:200), anti-ERG1/2/3 (SC-353, Santa Cruz; 1:100), goat anti mouse ESM1 (AF1999, R&D, 1:200), rabbit anti pMLC2 (3671T, Cell Signaling,1:200), rabbit anti mouse APOE (sc-6384, Santa Cruz, 1:200), rabbit anti mouse vWF (ab6994, Abcam, 1:200), rabbit anti mouse TXNRD1 (ab16840, Abcam, 1:200). The primary antibodies were detected using the appropriate Alexa 488, 594, or 647 secondary antibody conjugates (Invitrogen). For labeling of proliferating cells, mice were injected intraperitoneally with 20ul/g of EdU solution (1mg/ml, PBS) and sacrificed 3h later. EdU incorporation was visualized using the Click-iT EdU Cell Proliferation Kit (Thermo Fisher Scientific), according to the manufacturer's instructions.

Imaging and quantitative analysis—Samples were imaged using a confocal microscope (Zeiss LSM 770 or Zeiss LSM 800). Three-dimensional maximal projections were digitally constructed from confocal z-stacks. The images were edited using PhotoShop

software (CC2015, 22.00, Adobe) to optimize visualization. Quantifications were performed manually from microscopy images using Fiji software (Schindelin et al., 2012).

QUANTIFICATION AND STATISTICAL ANALYSIS

Statistical analysis—All graphs of quantitative data show mean values with SEM. In scatter plot graphs, each symbol represents one mouse, one retina or one image as indicated in the legends. All data were analyzed with Prism software using the Mann-Whitney U test, Kruskal Wallis test or 2-way ANOVA test. $P < 0.05$ was considered as statistically significant.

Supplementary Material

Refer to Web version on PubMed Central for supplementary material.

ACKNOWLEDGMENTS

We thank Dr. Bin Zhou from Shanghai Institutes for Biological Sciences for providing the *Mfsd2aCreER*^{T2} mice and Dr. Martin Matzuk from Baylor College of Medicine for providing the *Smad3*^{flox} mice. We thank Maxime Dubrac for helping us quantify OIR experiments. This work was supported by grants from the Canadian Institutes of Health Research (project grant PJT-165871), Vision Health Research Network (RRSV_PP1920), and AHA (17SDG3370 0124) to A.D., from the NIH (R01HL149343-01, 1R01EY025979-03, P30EY026878) and the Leducq Foundation (TNE ATTRACT) to A.E., and from EMBO (ALTF87-2016), NHLBI (2T32HL007974-16), and NEI (1K99E Y029375-01)to G.Z. X.X. was a recipient of a fellowship from the China Scholarship Council (CSC no. 201906285029).

REFERENCES

Adams RH, and Eichmann A (2010). Axon guidance molecules in vascular patterning. Cold Spring Harb. Perspect. Biol 2, a001875. [PubMed: 20452960]

Akhurst RJ, and Hata A (2012). Targeting the TGFbeta signalling pathway in disease. Nat. Rev. Drug Discov 11, 790–811. [PubMed: 23000686]

Allinson KR, Lee HS, Fruttiger M, Mccarty JH, and Arthur HM (2012). Endothelial expression of TGFbeta type II receptor is required to maintain vascular integrity during postnatal development of the central nervous system. PLoS One 7, e39336. [PubMed: 22745736]

Amano M, Ito M, Kimura K, Fukata Y, Chihara K, Nakano T, Matsuura Y, and Kaibuchi K (1996). Phosphorylation and activation of myosin by Rho-associated kinase (Rho-kinase). J. Biol. Chem 271, 20246–20249. [PubMed: 8702756]

Andreone BJ, Chow BW, Tata A, Lacoste B, Ben-Zvi A, Bullock K, Deik AA, Ginty DD, Clish CB, and Gu C (2017). Blood-brain barrier permeability is regulated by lipid transport-dependent suppression of caveolae-mediated transcytosis. Neuron 94, 581–594.e5. [PubMed: 28416077]

Armulik A, Genové G, and Betsholtz C (2011). Pericytes: developmental, physiological, and pathological perspectives, problems, and promises. Dev. Cell 21, 193–215. [PubMed: 21839917]

Armulik A, Genové G, Mäe M, Nisancioglu MH, Wallgard E, Niaudet C, He L, Norlin J, Lindblom P, Strittmatter K, et al. (2010). Pericytes regulate the blood-brain barrier. Nature 468, 557–561. [PubMed: 20944627]

Arnold TD, Ferrero GM, Qiu H, Phan IT, Akhurst RJ, Huang EJ, and Reichardt LF (2012). Defective retinal vascular endothelial cell development as a consequence of impaired integrin αVβ8-mediated activation of transforming growth factor-β. J. Neurosci 32, 1197–1206. [PubMed: 22279205]

Aspalter IM, Gordon E, Dubrac A, Ragab A, Narloch J, Vizán P, Geudens I, Collins RT, Franco CA, Abrahams CL, et al. (2015). Alk1 and Alk5 inhibition by Nrp1 controls vascular sprouting downstream of Notch. Nat. Commun 6, 7264. [PubMed: 26081042]

Augustin HG, and Koh GY (2017). Organotypic vasculature: From descriptive heterogeneity to functional pathophysiology. Science 357, eaal2379. [PubMed: 28775214]

Ben-Zvi A, Lacoste B, Kur E, Andreone BJ, Mayshar Y, Yan H, and Gu C (2014). Mfsd2a is critical for the formation and function of the blood-brain barrier. Nature 509, 507–511. [PubMed: 24828040]

Bernstein NJ, Fong NL, Lam I, Roy MA, Hendrickson DG, and Kelley DR (2020). Solo: doublet identification in single-cell RNA-seq via semi-supervised deep learning. Cell Syst. 11, 95–101.e5. [PubMed: 32592658]

Binet F, Cagnone G, Crespo-Garcia S, Hata M, Neault M, Dejda A, Wilson AM, Buscarlet M, Mawambo GT, Howard JP, et al. (2020). Neutrophil extracellular traps target senescent vasculature for tissue remodeling in retinopathy. Science 369, eaay5356. [PubMed: 32820093]

Blanco R, and Gerhardt H (2013). VEGF and Notch in tip and stalk cell selection. Cold Spring Harb. Perspect. Med 3, a006569. [PubMed: 23085847]

Chen J, Stahl A, Krah NM, Seaward MR, Joyal JS, Juan AM, Hatton CJ, Aderman CM, Dennison RJ, Willett KL, et al. (2012). Retinal expression of Wnt-pathway mediated genes in low-density lipoprotein receptor-related protein 5 (Lrp5) knockout mice. PLoS One 7, e30203. [PubMed: 22272305]

Chen PY, Qin L, Li G, Wang Z, Dahlman JE, Malagon-Lopez J, Gujja S, Cilfone NA, Kauffman KJ, Sun L, et al. (2019). Endothelial TGF-beta signalling drives vascular inflammation and atherosclerosis. Nat. Metab 1, 912–926. [PubMed: 31572976]

Chow BW, and Gu C (2017). Gradual suppression of transcytosis governs functional blood-retinal barrier formation. Neuron 93, 1325–1333.e3. [PubMed: 28334606]

Crist AM, Lee AR, Patel NR, Westhoff DE, and Meadows SM (2018). Vascular deficiency of Smad4 causes arteriovenous malformations: a mouse model of hereditary hemorrhagic telangiectasia. Angiogenesis 21, 363–380. [PubMed: 29460088]

De Bock K, Georgiadou M, Schoors S, Kuchnio A, Wong BW, Cantelmo AR, Quaegebeur A, Ghesquière B, Cauwenberghs S, Eelen G, et al. (2013). Role of PFKFB3-driven glycolysis in vessel sprouting. Cell 154, 651–663. [PubMed: 23911327]

Del Toro R, Prahst C, Mathivet T, Siegfried G, Kaminker JS, Larrivee B, Breant C, Duarte A, Takakura N, Fukamizu A, et al. (2010). Identification and functional analysis of endothelial tip cell-enriched genes. Blood 116, 4025–4033. [PubMed: 20705756]

Dubrac A, Künzel SE, Künzel SH, Li J, Chandran RR, Martin K, Greif DM, Adams RH, and Eichmann A (2018). NCK-dependent pericyte migration promotes pathological neovascularization in ischemic retinopathy. Nat. Commun 9, 3463. [PubMed: 30150707]

Dumas SJ, García-Caballero M, and Carmeliet P (2020). Metabolic signatures of distinct endothelial phenotypes. Trends Endocrinol. Metab 31, 580–595. [PubMed: 32622584]

Eilken HM, Diéguez-Hurtado R, Schmidt I, Nakayama M, Jeong HW, Arf H, Adams S, Ferrara N, and Adams RH (2017). Pericytes regulate VEGF-induced endothelial sprouting through VEGFR1. Nat. Commun 8, 1574. [PubMed: 29146905]

Finn RS, Dering J, Conklin D, Kalous O, Cohen DJ, Desai AJ, Ginther C, Atefi M, Chen I, Fowst C, et al. (2009). PD 0332991, a selective cyclin D kinase 4/6 inhibitor, preferentially inhibits proliferation of luminal estrogen receptor-positive human breast cancer cell lines in vitro. Breast Cancer Res. 11, R77. [PubMed: 19874578]

Gariano RF (2010). Special features of human retinal angiogenesis. Eye (Lond.) 24, 401–407. [PubMed: 20075971]

Gerhardt H, and Betsholtz C (2003). Endothelial-pericyte interactions in angiogenesis. Cell Tissue Res. 314, 15–23. [PubMed: 12883993]

Geudens I, and Gerhardt H (2011). Coordinating cell behaviour during blood vessel formation. Development 138, 4569–4583. [PubMed: 21965610]

Ghabrial AS, and Krasnow MA (2006). Social interactions among epithelial cells during tracheal branching morphogenesis. Nature 441, 746–749. [PubMed: 16760977]

Gilmour DF (2015). Familial exudative vitreoretinopathy and related retinopathies. Eye (Lond.) 29, 1–14. [PubMed: 25323851]

Hale P, Soliman SI, Sun H, and Lopez-Ramirez MA (2020). Isolation and purification of mouse brain endothelial cells to study cerebral cavernous malformation disease. Methods Mol. Biol 2152, 139–150. [PubMed: 32524550]

Hänzelmann S, Castelo R, and Guinney J (2013). GSVA: gene set variation analysis for microarray and RNA-seq data. BMC Bioinformatics 14, 7. [PubMed: 23323831]

Harada N, Tamai Y, Ishikawa T, Sauer B, Takaku K, Oshima M, and Taketo MM (1999). Intestinal polyposis in mice with a dominant stable mutation of the beta-catenin gene. EMBO J. 18, 5931–5942. [PubMed: 10545105]

Hirota S, Liu Q, Lee HS, Hossain MG, Lacy-Hulbert A, and Mccarty JH (2011). The astrocyte-expressed integrin αvβ8 governs blood vessel sprouting in the developing retina. Development 138, 5157–5166. [PubMed: 22069187]

Jakobsson L, Franco CA, Bentley K, Collins RT, Ponsioen B, Aspalter IM, Rosewell I, Busse M, Thurston G, Medvinsky A, et al. (2010). Endothelial cells dynamically compete for the tip cell position during angiogenic sprouting. Nat. Cell Biol 12, 943–953. [PubMed: 20871601]

Jeong HW, Hernández-Rodríguez B, Kim J, Kim KP, Enriquez-Gasca R, Yoon J, Adams S, Schöler HR, Vaquerizas JM, and Adams RH (2017). Transcriptional regulation of endothelial cell behavior during sprouting angiogenesis. Nat. Commun 8, 726. [PubMed: 28959057]

Ju W, Ogawa A, Heyer J, Nierhof D, Yu L, Kucherlapati R, Shafritz DA, and Böttinger EP (2006). Deletion of Smad2 in mouse liver reveals novel functions in hepatocyte growth and differentiation. Mol. Cell. Biol 26, 654–667. [PubMed: 16382155]

Junge HJ, Yang S, Burton JB, Paes K, Shu X, French DM, Costa M, Rice DS, and Ye W (2009). TSPAN12 regulates retinal vascular development by promoting Norrin- but not Wnt-induced FZD4/beta-catenin signaling. Cell 139, 299–311. [PubMed: 19837033]

Kureishi Y, Kobayashi S, Amano M, Kimura K, Kanaide H, Nakano T, Kaibuchi K, and Ito M (1997). Rho-associated kinase directly induces smooth muscle contraction through myosin light chain phosphorylation. J.Biol. Chem 272, 12257–12260. [PubMed: 9139666]

Larsson J, Goumans MJ, Sjöstrand LJ, Van Rooijen MA, Ward D, Levéen P, Xu X, Ten Dijke P, Mummery CL, and Karlsson S (2001). Abnormal angiogenesis but intact hematopoietic potential in TGF-beta type I receptor-deficient mice. EMBO J. 20, 1663–1673. [PubMed: 11285230]

Li Q, Pangas SA, Jorgez CJ, Graff JM, Weinstein M, and Matzuk MM (2008). Redundant roles of SMAD2 and SMAD3 in ovarian granulosa cells in vivo. Mol. Cell. Biol 28, 7001–7011. [PubMed: 18809571]

Liberzon A, Birger C, Thorvaldsdóttir H, Ghandi M, Mesirov JP, and Tamayo P (2015). The Molecular Signatures Database (MSigDB) hallmark gene set collection. Cell Syst. 1, 417–425. [PubMed: 26771021]

Liberzon A, Subramanian A, Pinchback R, Thorvaldsdóttir H, Tamayo P, and Mesirov JP (2011). Molecular signatures database (MSigDB) 3.0. Bioinformatics 27, 1739–1740. [PubMed: 21546393]

Luhmann UF, Lin J, Acar N, Lammel S, Feil S, Grimm C, Seeliger MW, Hammes HP, and Berger W (2005). Role of the Norrie disease pseudoglioma gene in sprouting angiogenesis during development of the retinal vasculature. Invest. Ophthalmol. Vis. Sci 46, 3372–3382. [PubMed: 16123442]

Lun ATL, Riesenfeld S, Andrews T, Dao TP, Gomes T; participants in the 1st Human Cell Atlas Jamboree, and Marioni JC (2019). EmptyDrops: distinguishing cells from empty droplets in droplet-based single-cell RNA sequencing data. Genome Biol. 20, 63. [PubMed: 30902100]

Macosko EZ, Basu A, Satija R, Nemesh J, Shekhar K, Goldman M, Tirosh I, Bialas AR, Kamitaki N, Martersteck EM, et al. (2015). Highly parallel genome-wide expression profiling of individual cells using nanoliter droplets. Cell 161, 1202–1214. [PubMed: 26000488]

Mäe MA, He L, Nordling S, Vazquez-Liebanas E, Nahar K, Jung B, Li X, Tan BC, Chin Foo J, Cazenave-Gassiot A, et al. (2021). Single-cell analysis of blood-brain barrier response to pericyte loss. Circ. Res 128, e46–e62. [PubMed: 33375813]

Massagué J (2012). TGFbeta signalling in context. Nat. Rev. Mol. Cell Biol 13, 616–630. [PubMed: 22992590]

Mazzoni J, Smith JR, Shahriar S, Cutforth T, Ceja B, and Agalliu D (2017).The Wnt inhibitor Apcdd1 coordinates vascular remodeling and barrier maturation of retinal blood vessels. Neuron 96, 1055–1069.e6. [PubMed: 29154126]

Milde F, Lauw S, Koumoutsakos P, and Iruela-Arispe ML (2013). The mouse retina in 3D: quantification of vascular growth and remodeling. Integr. Biol. (Camb) 5, 1426–1438. [PubMed: 24136100]

Miller JW, LeCouter J, Strauss EC, and Ferrara N (2013).Vascular endothelial growth factor A in intraocular vascular disease. Ophthalmology 120, 106–114. [PubMed: 23031671]

Morgan M, Pagès H, Obenchain V, and Hayden N (2021). Rsamtools: Binary alignment (BAM), FASTA, variant call (BCF), and tabix file import (R package version 2.8.0). https://bioconductor.org/packages/Rsamtools.

Muzumdar MD, Tasic B, Miyamichi K, Li L, and Luo L (2007). A global double-fluorescent Cre reporter mouse. Genesis 45, 593–605. [PubMed: 17868096]

Ola R, Dubrac A, Han J, Zhang F, Fang JS, Larrivée B, Lee M, Urarte AA, Kraehling JR, Genet G, et al. (2016). PI3 kinase inhibition improves vascular malformations in mouse models of hereditary haemorrhagic telangiectasia. Nat. Commun 7, 13650. [PubMed: 27897192]

Ola R, Künzel SH, Zhang F, Genet G, Chakraborty R, Pibouin-Fragner L, Martin K, Sessa W, Dubrac A, and Eichmann A (2018). SMAD4 prevents flow induced arteriovenous malformations by inhibiting casein kinase 2. Circulation 138, 2379–2394. [PubMed: 29976569]

Park DY, Lee J, Kim J, Kim K, Hong S, Han S, Kubota Y, Augustin HG, Ding L, Kim JW, et al. (2017). Plastic roles of pericytes in the blood-retinal barrier. Nat. Commun 8, 15296. [PubMed: 28508859]

Potente M, Gerhardt H, and Carmeliet P (2011). Basic and therapeutic aspects of angiogenesis. Cell 146, 873–887. [PubMed: 21925313]

Potente M, and Mäkinen T (2017). Vascular heterogeneity and specialization in development and disease. Nat. Rev. Mol. Cell Biol 18, 477–494. [PubMed: 28537573]

Pu W, He L, Han X, Tian X, Li Y, Zhang H, Liu Q, Huang X, Zhang L, Wang Q-D, et al. (2018). Genetic targeting of organ-specific blood vessels. Circ. Res 123, 86–99. [PubMed: 29764841]

Rapaport DH, Wong LL, Wood ED, Yasumura D, and Lavail MM (2004). Timing and topography of cell genesis in the rat retina. J. Comp. Neurol 474, 304–324. [PubMed: 15164429]

Rocha SF, Schiller M, Jing D, Li H, Butz S, Vestweber D, Biljes D, Drexler HC, Nieminen-Kelhä M, Vajkoczy P, et al. (2014). Esm1 modulates endothelial tip cell behavior and vascular permeability by enhancing VEGF bioavailability. Circ. Res 115, 581–590. [PubMed: 25057127]

Sapieha P, Joyal JS, Rivera JC, Kermorvant-Duchemin E, Sennlaub F, Hardy P, Lachapelle P, and Chemtob S (2010). Retinopathy of prematurity: understanding ischemic retinal vasculopathies at an extreme of life. J. Clin. Invest 120, 3022–3032. [PubMed: 20811158]

Schindelin J, Arganda-Carreras I, Frise E, Kaynig V, Longair M, Pietzsch T, Preibisch S, Rueden C, Saalfeld S, Schmid B, et al. (2012). Fiji: an open-source platform for biological-image analysis. Nat. Methods 9, 676–682. [PubMed: 22743772]

Schoors S, Bruning U, Missiaen R, Queiroz KC, Borgers G, Elia I, Zecchin A, Cantelmo AR, Christen S, Goveia J, et al. (2015). Fatty acid carbon is essential for dNTP synthesis in endothelial cells. Nature 520, 192–197. [PubMed: 25830893]

Shi Y, and Massagué J (2003). Mechanisms of TGF-beta signaling from cell membrane to the nucleus. Cell 113, 685–700. [PubMed: 12809600]

Stahl A, Connor KM, Sapieha P, Chen J, Dennison RJ, Krah NM, Seaward MR, Willett KL, Aderman CM, Guerin KI, et al. (2010). The mouse retina as an angiogenesis model. Invest. Ophthalmol. Vis. Sci 51, 2813–2826. [PubMed: 20484600]

Strasser GA, Kaminker JS, and Tessier-Lavigne M (2010). Microarray analysis of retinal endothelial tip cells identifies CXCR4 as a mediator of tip cell morphology and branching. Blood 115, 5102–5110. [PubMed: 20154215]

Stuart T, Butler A, Hoffman P, Hafemeister C, Papalexi E, Mauck WM 3rd, Hao Y, Stoeckius M, Smibert P, and Satija R (2019). Comprehensive integration of single-cell data. Cell 177, 1888–1902.e21. [PubMed: 31178118]

Subramanian A, Tamayo P, Mootha VK, Mukherjee S, Ebert BL, Gillette MA, Paulovich A, Pomeroy SL, Golub TR, Lander ES, and Mesirov JP (2005). Gene set enrichment analysis: a knowledge-based approach for interpreting genome-wide expression profiles. Proc. Natl. Acad. Sci. USA 102, 15545–15550. [PubMed: 16199517]

Tiriac A, Smith BE, and Feller MB (2018). Light prior to eye opening promotes retinal waves and eye-specific segregation. Neuron 100, 1059–1065.e4. [PubMed: 30392793]

Totsukawa G, Yamakita Y, Yamashiro S, Hartshorne DJ, Sasaki Y, and Matsumura F (2000). Distinct roles of ROCK (Rho-kinase) and MLCK in spatial regulation of MLC phosphorylation for assembly of stress fibers and focal adhesions in 3T3 fibroblasts. J. Cell Biol 150, 797–806. [PubMed: 10953004]

Tual-Chalot S, Mahmoud M, Allinson KR, Redgrave RE, Zhai Z, Oh SP, Fruttiger M, and Arthur HM (2014). Endothelial depletion of Acvrl1 in mice leads to arteriovenous malformations associated with reduced endoglin expression. PLoS One 9, e98646. [PubMed: 24896812]

Ventura A, Kirsch DG, Mclaughlin ME, Tuveson DA, Grimm J, Lintault L, Newman J, Reczek EE, Weissleder R, and Jacks T (2007). Restoration of p53 function leads to tumour regression in vivo. Nature 445, 661–665. [PubMed: 17251932]

Wang Y, Nakayama M, Pitulescu ME, Schmidt TS, Bochenek ML, Sakakibara A, Adams S, Davy A, Deutsch U, Lüthi U, et al. (2010). Ephrin-B2 controls VEGF-induced angiogenesis and lymphangiogenesis. Nature 465, 483–486. [PubMed: 20445537]

Wang Z, Liu CH, Huang S, Fu Z, Tomita Y, Britton WR, Cho SS, Chen CT, Sun Y, Ma J-X, et al. (2020). Wnt signaling activates MFSD2A to suppress vascular endothelial transcytosis and maintain blood-retinal barrier. Sci. Adv 6, eaba7457. [PubMed: 32923627]

Weiner GA, Shah SH, Angelopoulos CM, Bartakova AB, Pulido RS, Murphy A, Nudleman E, Daneman R, and Goldberg JL (2019). Cholinergic neural activity directs retinal layer-specific angiogenesis and blood retinal barrier formation. Nat. Commun 10, 2477. [PubMed: 31171770]

Xia CH, Liu H, Cheung D, Wang M, Cheng C, Du X, Chang B, Beutler B, and Gong X (2008). A model for familial exudative vitreoretinopathy caused by LPR5 mutations. Hum. Mol. Genet 17, 1605–1612. [PubMed: 18263894]

Xu Q, Wang Y, Dabdoub A, Smallwood PM, Williams J, Woods C, Kelley MW, Jiang L, Tasman W, Zhang KJ, and Nathans J (2004). Vascular development in the retina and inner ear: control by Norrin and Frizzled-4, a high-affinity ligand-receptor pair. Cell 116, 883–895. [PubMed: 15035989]

Yang X, Li C, Herrera PL, and Deng CX (2002). Generation of Smad4/Dpc4 conditional knockout mice. Genesis 32, 80–81. [PubMed: 11857783]

Ye X, Wang Y, Cahill H, Yu M, Badea TC, Smallwood PM, Peachey NS, and Nathans J (2009). Norrin, frizzled-4, and Lrp5 signaling in endothelial cells controls a genetic program for retinal vascularization. Cell 139, 285–298. [PubMed: 19837032]

Zhang YE (2017). Non-Smad signaling pathways of the TGF-beta family. Cold Spring Harb. Perspect. Biol 9, a022129. [PubMed: 27864313]

Zhao Q, Eichten A, Parveen A, Adler C, Huang Y, Wang W, Ding Y, Adler A, Nevins T, and Ni M (2018). Single- cell transcriptome analyses reveal endothelial cell heterogeneity in tumors and changes following antiangiogenic treatment. Cancer Res. 78, 2370–2382. [PubMed: 29449267]

Highlights

- scRNA-seq identifies two distinct tip cell populations guiding retina vascularization
- D-tip cells diving into the neuroretina have a distinct molecular signature
- Non-canonical TGF-β signaling is essential for D-tip cell specification
- Tip endothelial cell gene expression profiles are altered in ischemic retinopathy

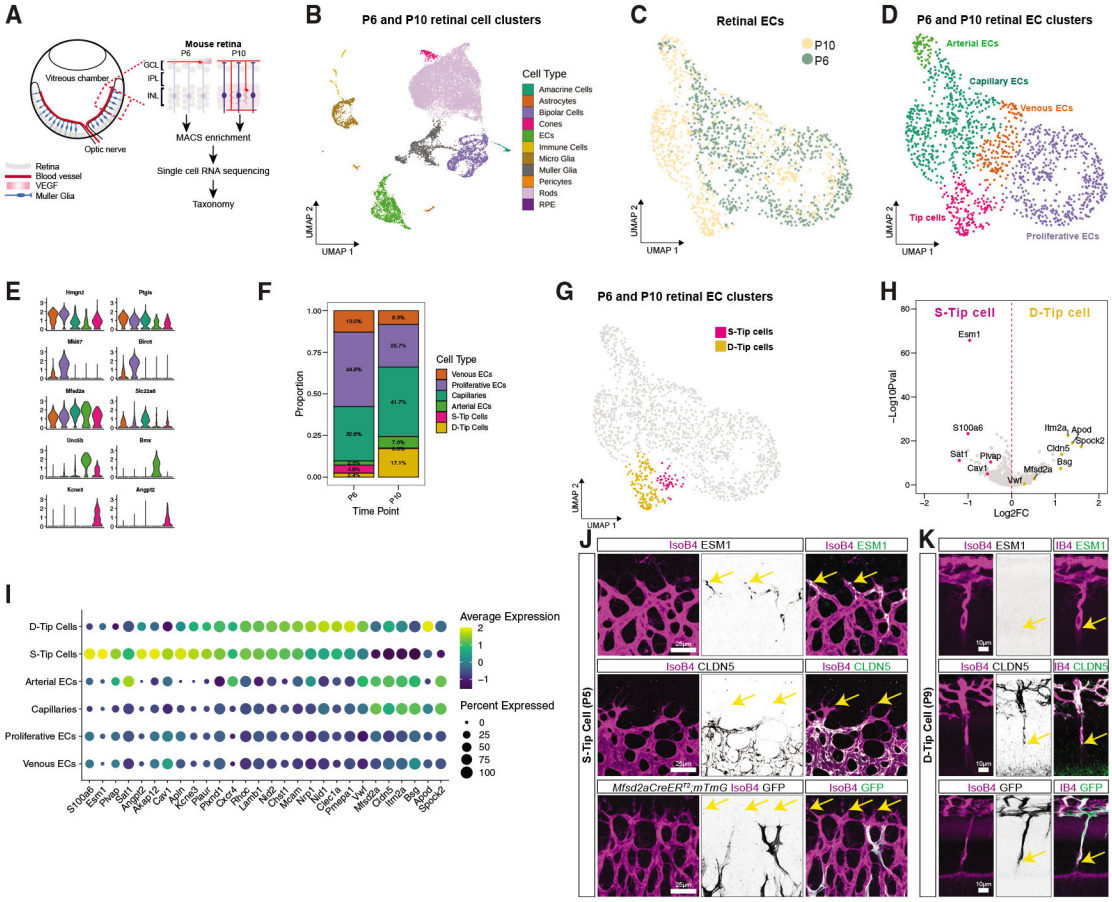

Figure 1. Identification of temporal retinal EC heterogeneity

(A) scRNA-seq experimental design.

(B) UMAP plot of retinal cells from P6 and P10 retinas.

(C) UMAP plot of ECs from P6 and P10 retinas.

(D) UMAP plot of EC sub-clusters from P6 and P10 retinas.

(E) Violin plots of the expression of endothelial sub-cluster markers.

(F) Relative fraction of EC sub-clusters in P6 and P10 retinas.

(G) UMAP plot of tip cell sub-clustering in the integrated P6 and P10 datasets.

(H) Volcano plot of differentially expressed genes between S- and D-tip cells.

(I) Dot plot of expression level and frequency among cell clusters of selected genes in all P6 and P10 ECs. Color scale: yellow, high expression; dark blue, low expression.

(J and K) Double IsoB4/ESM1 and PECAM1/CLDN5 immunostaining of WT retina, and IsoB4/GFP double staining of *Mfsd2aCreER^{T2};mTmG* retina at P5 and P9.

(J) P5 flat-mounted retina, view from the top, (K) P9 retina cross-sections.

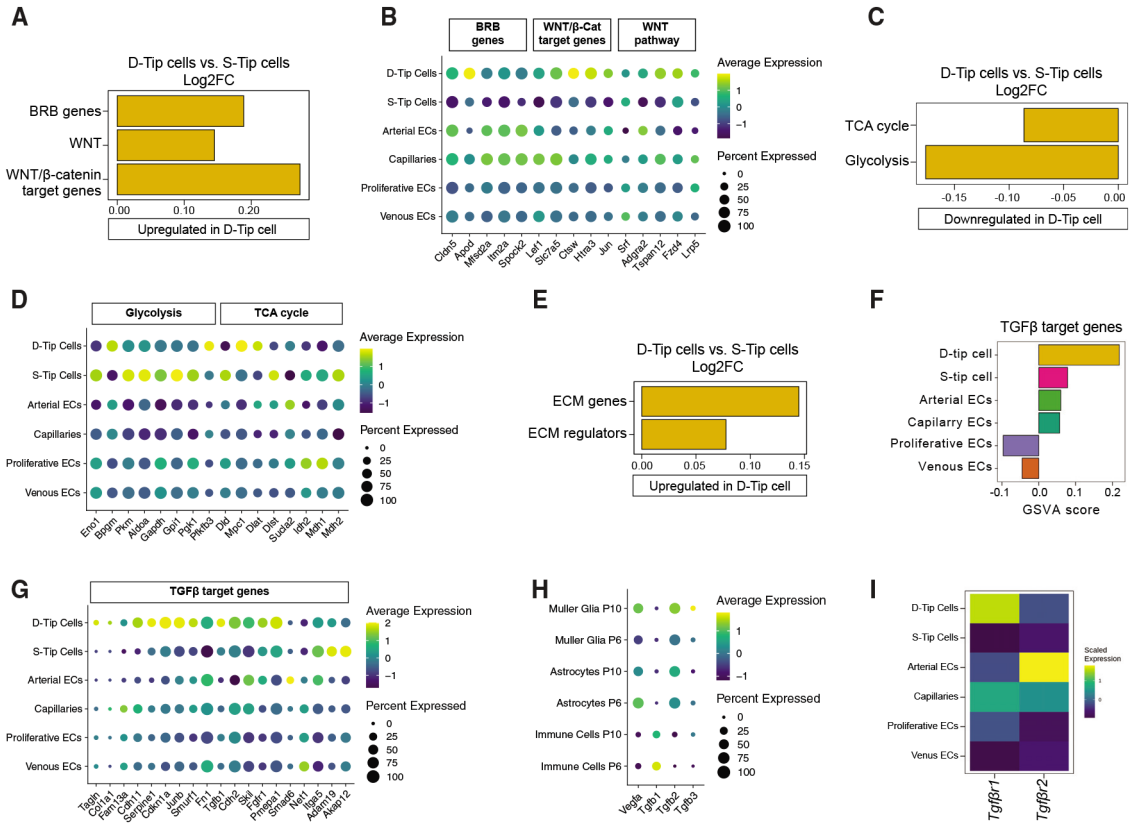

Figure 2. Characterization of specialized neuroretina D-tip cells

(A) Gene set signatures involved in BRB and WNT signaling represented by $\log_2$ fold change of GSVA score comparing transcripts from P6 and P10 tip cells.

(B) Dot plot of expression level and frequency among cell clusters of selected genes in all P6 and P10 ECs.

(C) Gene set signatures involved in glycolysis and TCA cycle comparing transcripts from P6 and P10 tip cells.

(D) Dot plot of expression level and frequency among cell clusters of selected genes in all P6 and P10 ECs.

(E) Gene set signatures of ECM and ECM regulators comparing transcripts from P6 and P10 tip cells.

(F) Gene set signatures for TGF-β target genes represented by GSVA score for each retinal EC cluster.

(G) Dot plot of expression level and frequency among cell clusters of selected genes in all P6 and P10 ECs.

(H) Dot plot of expression level and frequency among cell clusters of selected genes in P6 or P10 ECs.

(I) Heatmap showing *Tgfβr1* and *Tgfβr2* expression levels in all P6 and P10 EC clusters.

In (B, D, G, H, and I) color scale: yellow, high expression; dark blue, low expression.

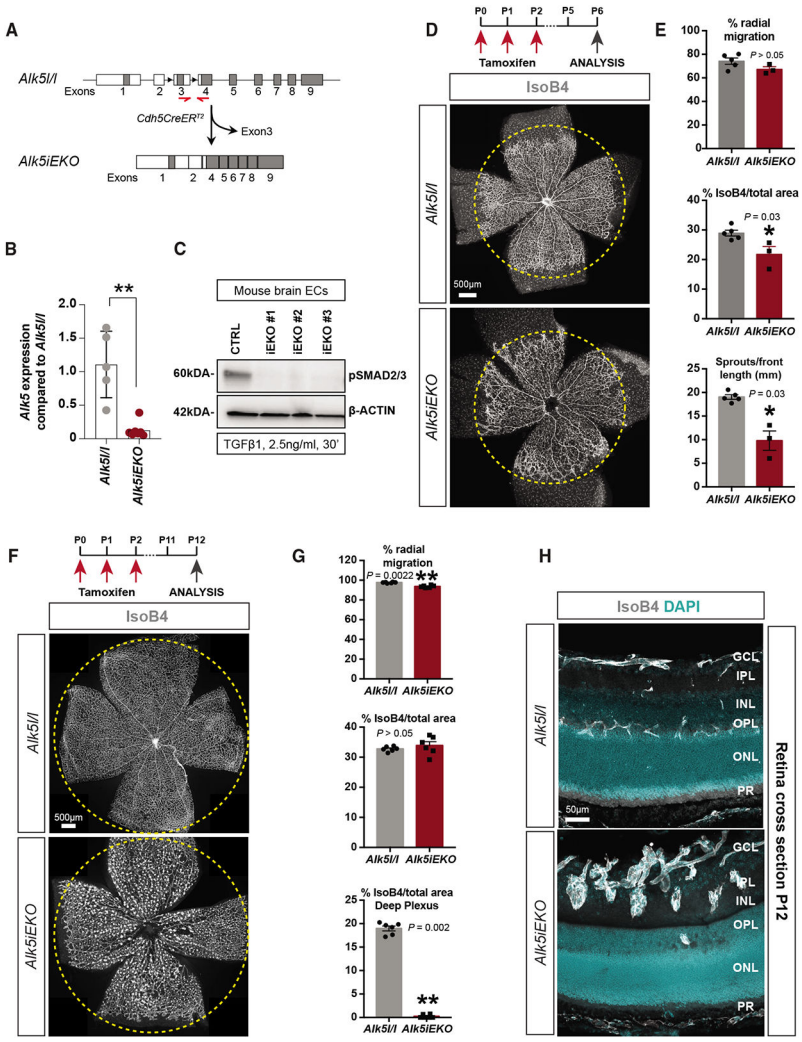

Figure 3. Endothelial TGF-β signaling is essential for neuroretina vascularization

(A) Experimental strategy to delete *Alk5* in ECs. Red arrows indicate the qPCR primer hybridization sites.

(B) qPCR measurement of *Alk5* levels in *Alk5l/l* and *Alk5iEKO* mouse brain ECs (mean ± SEM, each dot represents one mouse, **p < 0.01, Mann-Whitney U test).

(C) Western blot for phospho-SMAD2/3, and β-actin using CTRL (*Alk5l/l*) and *Alk5iEKO* mouse brain ECs treated for 30 min with TGF-β1.

(D) Top, experimental strategy to assess retinal vascularization at P6. Red arrows indicate TAM injections. Bottom, IsoB4 staining of retinal flat mounts.

(E) Quantification of vascular parameters of *Alk5l/l* and *Alk5iEKO* P6 retinas (mean ± SEM, each dot represents one retina, *p < 0.05, Mann-Whitney U test).

(F) Top, experimental strategy to assess retinal vascularization at P12. Red arrows indicate TAM injections. Bottom, IsoB4 staining of retinal flat mounts.

(G) Quantification of vascular parameters of *Alk5l/l* and *Alk5iEKO* P12 retinas (mean ± SEM, each dot represents one retina, **p < 0.01, Mann-Whitney U test).

(H) IsoB4 and DAPI double staining of P12 *Alk5l/l* and *Alk5iEKO* retina cross-sections. GCL, ganglion cell layer; IPL, inner plexiform layer; INL, inner nuclear layer; OPL, outer plexiform layer; ONL, outer nuclear layer; PR, photoreceptors.

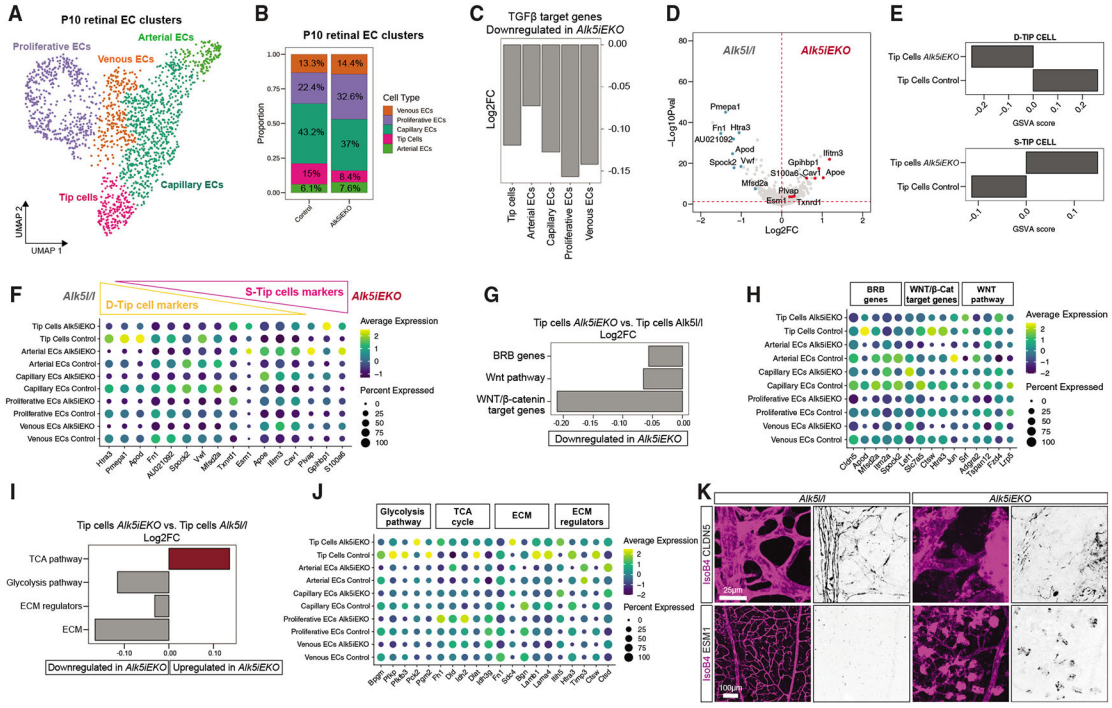

Figure 4. Characterization of *Alk5iEKO* tip cells

(A) UMAP plot of EC sub-clusters from P10 *Alk5l/l* and *Alk5iEKO* retinas.

(B) Relative proportions of EC sub-clusters in *Alk5l/l* and *Alk5iEKO* retinas.

(C) TGF-β target gene signatures of *Alk5iEKO* compared with *Alk5l/l* ECs at P10.

(D) Volcano plot of differentially expressed genes between *Alk5iEKO* and *Alk5l/l* ECs at P10.

(E) Gene set signatures involved in D- and S-tip cell identity comparing transcripts from *Alk5iEKO* and *Alk5l/l* P10 ECs.

(F) Dot plot of expression level and frequency of selected genes among cell clusters in P10 *Alk5iEKO* and *Alk5l/l* ECs.

(G) Gene set signatures involved in BRB and WNT signaling comparing transcripts from P10 *Alk5iEKO* and *Alk5l/l* tip ECs.

(H) Dot plot of expression level and frequency of selected genes among cell clusters in P10 *Alk5iEKO* and *Alk5l/l* ECs.

(I) Gene set signatures involved in glycolysis and TCA cycle comparing transcripts of *Alk5iEKO* and *Alk5l/l* tip ECs at P10.

(J) Dot plot of expression level and frequency of selected genes among clusters in P10 *Alk5iEKO* and *Alk5l/l* ECs.

(K) IsoB4/CLDN5 (top) or IsoB4/ ESM1 (bottom) double staining of P12 *Alk5l/l* and *Alk5iEKO* retina flat mounts.

In (F), (H), and (J) color scale: yellow, high expression; dark blue, low expression.

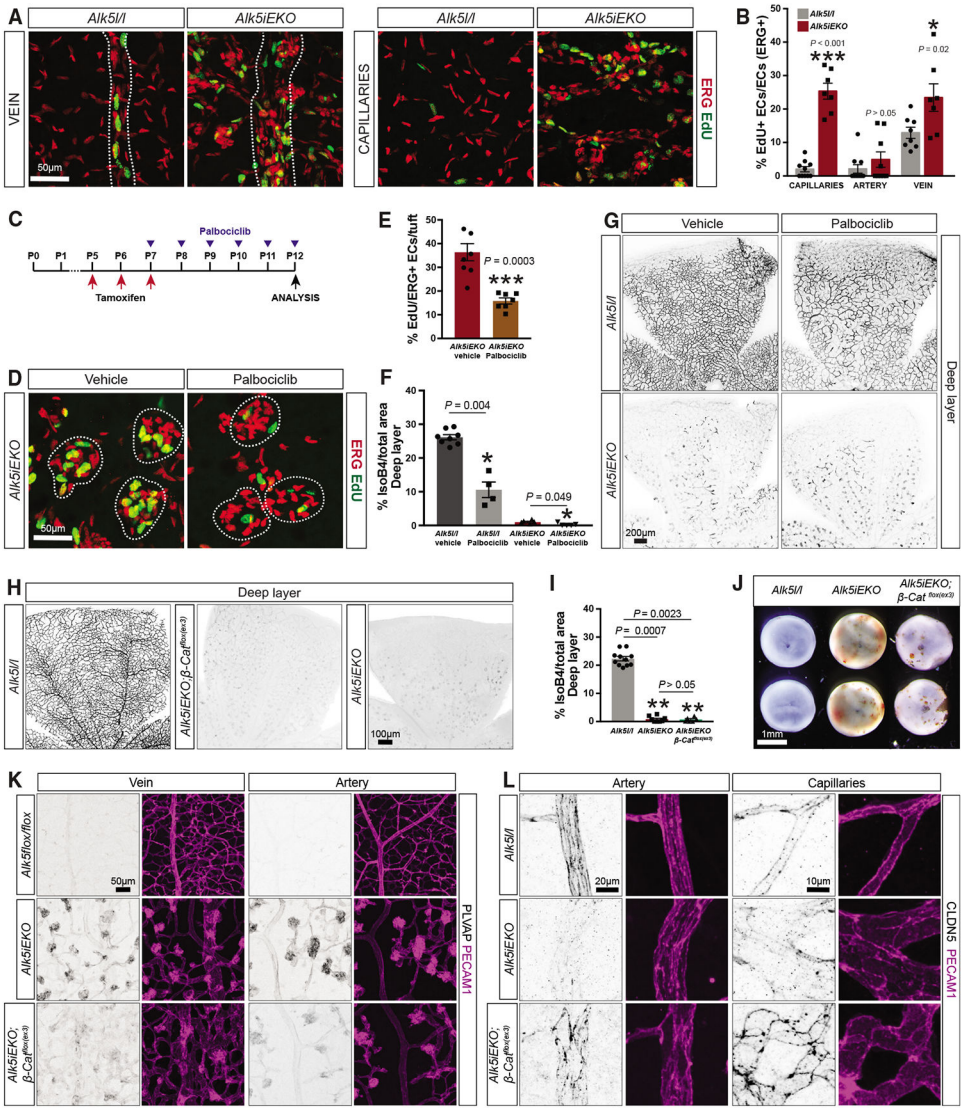

Figure 5. Inhibition of proliferation and WNT overactivation in *Alk5iEKOs*

(A) EdU and ERG1/2/3 double staining of vein (left) and capillaries (right) from P12 retinas.

(B) Quantification of EdU+;ERG1/2/3+ ECs in P12 *Alk5l/l* and *Alk5iEKO* retinas (mean ± SEM, each dot represents one retina, *p < 0.05, ***p < 0.001, Mann-Whitney U test).

(C) Experimental strategy to inhibit proliferation. Red arrows indicate TAM injections, and blue arrowheads indicate Palbociclib injections (50 μg/g).

(D) EdU and ERG1/2/3 double staining of *Alk5iEKO* tufts treated with vehicle or Palbociclib.

(E) Quantification of EdU+ ERG1/2/3+ ECs in *Alk5iEKO* tufts treated with vehicle or Palbociclib (mean ± SEM, each dot represents one retina, ***p < 0.001, Mann-Whitney U test).

(F) Quantification of IsoB4+ deep vascular plexus area from control and *Alk5iEKO* mice treated with vehicle or Palbociclib (mean ± SEM, each dot represents one retina, *p < 0.05, Mann-Whitney U test).

(G) IsoB4 staining of deep vascular plexus from control and *Alk5iEKO* mice treated with vehicle or Palbociclib.

(H) IsoB4 staining of deep vascular plexus from P12 control, *Alk5iEKO*, and *Alk5iEKO;β-Catenin*$^{flox(ex3)}$ mice.

(I) Quantification of IsoB4+ deep vascular plexus area from the retinas shown in (H) (mean ± SEM, each dot represents one retina, **p < 0.005, Kruskal Wallis test).

(J) Freshly dissected P12 retinas from *Alk5l/l, Alk5iEKO*, and *Alk5iEKO;β-Catenin*$^{flox(ex3)}$ mice to visualize hemorrhage.

(K) PECAM1/PLVAP double staining of P12 retina flat mounts of the indicated genotypes.

(L) PECAM1/CLDN5 double staining of P12 retinas of the indicated genotypes.

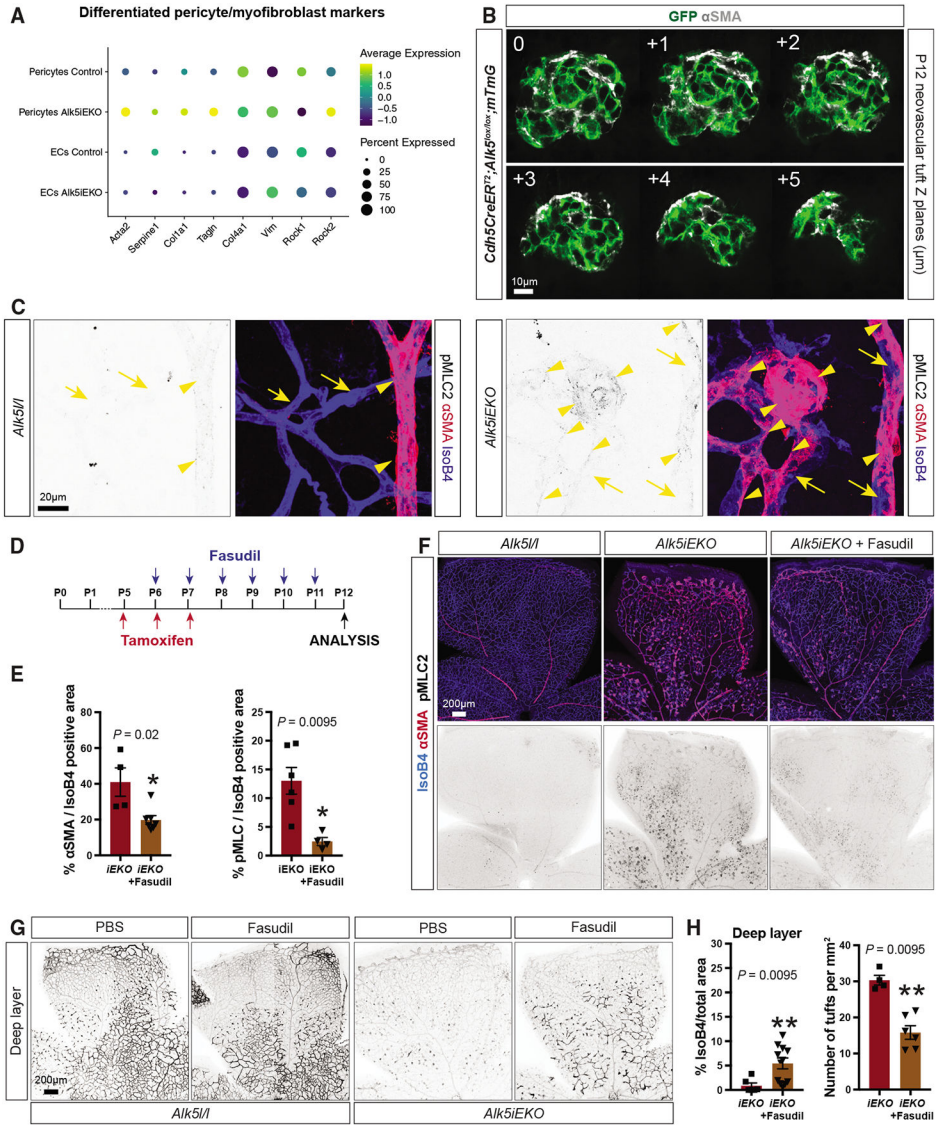

Figure 6. ALK5 inhibition promotes mural cell dysfunction

(A) Dot plot of expression level and frequency of selected genes among EC and pericyte clusters from *Alk5l/l* and *Alk5iEKO* P10 retinas. Color scale: yellow, high expression; dark blue, low expression.

(B) Sequential optical cross-sections of NVTs from *Alk5iEKO;mTmG* mice stained for α-SMA and GFP.

(C) IsoB4/α-SMA/p-MLC2 triple staining of P12 retinas of the indicated genotypes. Arrows point toward IsoB4+;α-SMA−;pMLC2− areas and arrowheads point toward IsoB4+;α-SMA+;pMLC2+ areas.

(D) Experimental strategy to inhibit ROCK signaling. Red arrows indicate TAM injections and blue arrows indicate Fasudil injections.

(E) Quantification of α-SMA+ and pMLC2+ area from P12 *Alk5iEKO* mice treated with vehicle or Fasudil (mean ± SEM, each dot represents one retina, *p < 0.05, Mann-Whitney U test).

(F) IsoB4/α-SMA/p-MLC2 triple staining of P12 retinas of the indicated genotypes, treated according to (D).
(G) IsoB4 staining of deep vascular plexus from P12 control and *Alk5iEKO* mice treated according to (D).
(H) Quantification of IsoB4+ deep vascular plexus area from P12 *Alk5iEKO* mice treated with vehicle or Fasudil (mean ± SEM, each dot represents one retina, **p < 0.01, Mann-Whitney U test).

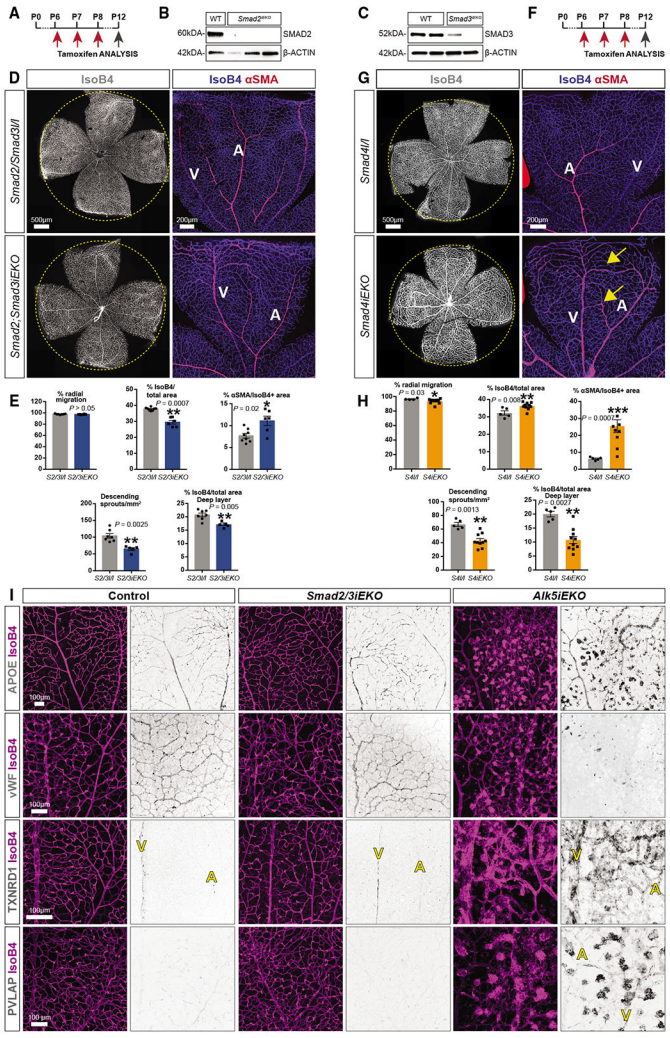

Figure 7. Effects of endothelial *Smad* deletion on retinal vasculature

(A) Experimental strategy to delete *Smad2* and *Smad3* in ECs. Red arrows indicate TAM injections.

(B and C) Western blot for SMAD2 or SMAD3 and β-actin using ECs isolated from lungs of WT (*Smad2l/l* or *Smad3l/l*) and *Smad2iEKO* and *Smad3iEKO* mice, respectively.

(D) IsoB4/α-SMA double staining of P12 retinas of the indicated genotypes.

(E) Quantification of vascular parameters of *Smad2/3l/l* and *Smad2/3iEKO* P12 retinas (mean ± SEM, each dot represents one retina, *p < 0.05, **p < 0.01, Mann-Whitney U test).

(F) Experimental strategy to delete *Smad4* in ECs. Red arrows indicate TAM injections.

(G) IsoB4 and α-SMA double staining of P12 *Smad4l/l* and *Smad4iEKO* retinas.

(H) Quantification of vascular parameters of P12 retinas of the indicated genotypes (mean ± SEM, each dot represents one retina, *p < 0.05, **p < 0.01, **p < 0.001, Mann-Whitney U test).

(I) Double immunostainings for IsoB4 and APOE, VWF, TXNDR1, or PLVAP of retina flat mounts of the indicated genotypes at P12. A, artery; V, vein.

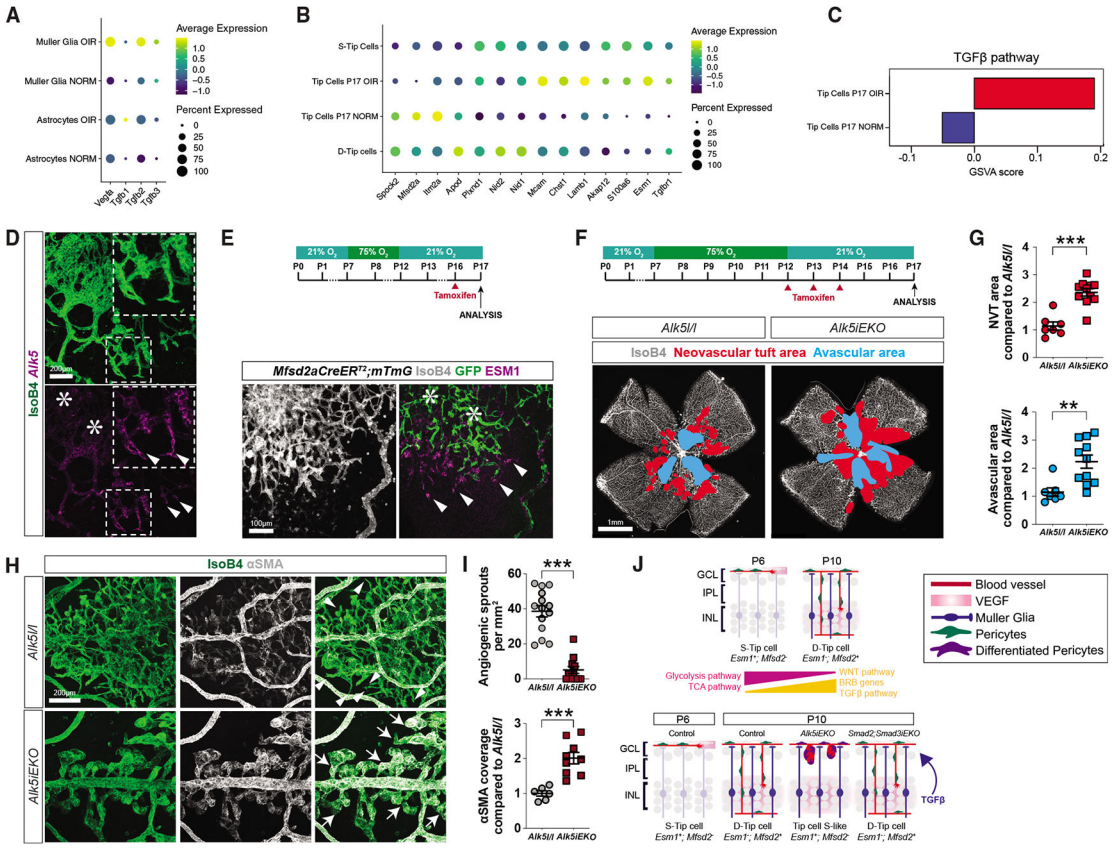

Figure 8. Endothelial TGF-β signaling promotes retinal revascularization in OIR

(A) Dot plot of *Tgfβ1, Tgfβ2, Tgfβ3*, and *Vegf* expression by Müller glia and astrocytes from P17 normoxia and OIR retinas.

(B) Dot plot of expression level and frequency of tip cell markers among clusters of P6 S-tip cells and P10 D-tip cells, and P17 normoxia and OIR tip cells.

(C) Gene set signatures involved in TGF-β signaling for P17 normoxia and OIR tip cells.

(D) *Alk5* mRNA labeling in OIR retinas by fluorescence ISH using RNAscope. Arrowheads point to revascularizing sprouts and asterisks point to NVTs.

(E) Top, strategy for genetic labeling of MFSD2A+ cells by TAM treatment (red arrowhead) using *Mfsd2aCreER^{T2};mTmG* mice subjected to OIR. Bottom, IsoB4/GFP/ESM1 triple staining of OIR retinas from P17 *Mfsd2aCreER^{T2};mTmG* mice.

(F) Top, experimental strategy to delete endothelial *Alk5* during OIR. Red arrowheads indicate TAM injections. Bottom, IsoB4 staining of P17 OIR retinas of the indicated genotypes. Avascular area is shown in blue and NVT area is shown in red.

(G) Quantification of avascular area and NVT area of P17 *Alk5l/l and Alk5iEKO* OIR retinas (mean ± SEM, each dot represents one retina, **p < 0.01, ***p < 0.001, Mann-Whitney U test).

(H) IsoB4/α-SMA double staining of P17 *Alk5l/l* and *Alk5iEKO* OIR retinas. Arrowheads point to revascularizing sprouts and arrows point to NVTs.

(I) Quantification of angiogenic sprouts, and α-SMA coverage of P17 OIR retinas of the indicated genotypes (mean ± SEM, each dot represents one image from at least 4 retinas per condition, ***p < 0.001, Mann-Whitney U test).

(J) Top, summary of transcriptional changes in tip cells between P6 and P10. Bottom, working model for TGF-β-induced D-tip cell differentiation and neuroretina vascularization. In (A and B) color scale: yellow, high expression; dark blue, low expression.

KEY RESOURCES TABLE

REAGENT or RESOURCE	SOURCE	IDENTIFIER
Antibodies		
Anti-Actin, α-Smooth Muscle - Cy3™ antibody, Mouse monoclonal, clone 1A4	Sigma-Aldrich	Cat#C6198; RRID: AB_476856
Mouse/Rat CD31/PECAM-1 antibody, Polyclonal Goat IgG	R&D Systems	Cat#AF3628; RRID: AB_2161028
GFP Recombinant Rabbit Monoclonal Antibody, Rabbit / IgG	Invitrogen	Cat#G10362; RRID: AB_2536526
Rat Anti-Mouse Panendothelial Cell Antigen Clone MECA-32	BD Pharmingen	Cat#553849; RRID: AB_395086
Claudin 5 Polyclonal Antibody, Rabbit / IgG	Invitrogen	Cat#34-1600; RRID: AB_2533157
Mouse DLL4 Antibody, Polyclonal Goat IgG	R&D Systems	Cat#AF1389; RRID: AB_354770
Erg-1/2/3 Antibody (C-20), Rabbit Polyclonal IgG	Santa Cruz Biotechnology	Cat#SC-353; RRID: AB_675518
Mouse Endocan/ESM-1 Antibody, Polyclonal Goat IgG	R&D Systems	Cat#AF1999; RRID: AB_2101810
Phospho-Myosin Light Chain 2 (Ser19) Antibody, rabbit	Cell Signaling	Cat#3671T; RRID: AB_330248
apoE (M-20): sc-6384, goat polyclonal antibody	Santa Cruz Biotechnology	Cat#sc-6384; RRID: AB_634036
Anti-Von Willebrand Factor antibody, Rabbit polyclonai IgG	Abcam	Cat#ab6994; RRID: AB_305689
Anti-TXNRD1 antibody, rabbit polyclonal IgG	Abcam	Cat#ab16840; RRID: AB_2210118
Alexa Fluor® (H+L) cross-absorbedsecondary antibodies	Invitrogen	https://www.thermofisher.com/antibody/secondary/query/alexa
Rabbit Anti-Smad3 (C67H9) monoclonal antibody	Cell Signaling	Cat#9523; RRID: AB_2193182
Rabbit anti-Smad2 (D43B4) XP® monoclonal antibody	Cell Signaling	Cat#5339; RRID: AB_10626777
Anti-p-SMAD2/3	Cell Signaling	Cat#8828; RRID: AB_2631089
Anti-β-actin	Sigma-Aldrich	Cat#A1978; RRID: AB_476692
Chemicals, peptides, and recombinant proteins		
Tamoxifen	Sigma-Aldrich	Cat#T5648; CAS: 10540-29-1
Fasudil-Hydrochloride	Sigma-Aldrich	Cat#CDS021620
PD 0332991 isethionate (Palbociclib)	Sigma-Aldrich	Cat#PZ0199; CAS: 827022-33-3
Formaldehyde	Sigma-Aldrich	Cat#F8775; CAS: 50-00-0
Phosphate Buffered Saline	DOT SCIENTIFIC INC	Cat#DSP32080-100T
UltraPure™ Low Melting Point Agarose	Thermo-Fisher Scientific	Cat#16520100
Tissue-Plus™ O.C.T. Compound Tissue-Plus™	Fisher Scientific	Cat#23-730-571
Bovine serum albumin	AmericanBIO	Cat#ab01088
Fetal Bovine Serum	Gibco (Thermo-Fisher Scientific)	Cat#16140-071
Fluorescence Mounting Medium	Agilent (Dako)	Cat#S302380-2
VECTASHIELD® Antifade Mounting Medium with DAPI	Vector Laboratories	Cat#H-1200-10
Isolectin GS-IB4 from Griffonia simplicifolia, Alexa Fluor™ 488 Conjugate	Invitrogen	Cat#I21411
Mitomycin C	Fisher Scientific	Cat#AC226940020; CAS: 50-07-7, 7647-14-5
EGM2	Lonza	Cat#CC-3162
4-hydroxy-tamoxifen	Sigma-Aldrich	Cat#H7904
penicillin-streptomycin	Thermo-Fisher Scientific	Cat#15070063
bovine serum albumin	Fisher Scientific	Cat#BP1600

REAGENT or RESOURCE	SOURCE	IDENTIFIER
Dulbecco's modified Eagle medium	Thermo-Fisher Scientific	Cat#10569044
collagenase/dispase	Sigma-Aldrich	Cat#10269638001
DNase I	Sigma-Aldrich	Cat#11284932001
DNase I	Qiagen	Cat#79254
tosyl-lysine-chloromethyl-ketone	Sigma-Aldrich	Cat#T7254
TGFβ1	Cell signaling	Cat#8915
N-2-hydroxyethylpiperazine-*N*′-2-ethanesulfonic acid	Thermo-Fisher Scientific	Cat#15630080
Immobilon ECL Ultra Western HRP Substrate	Millipore	Cat#WBKLS0500
Critical commercial assays		
RNeasy Plus Mini Kit	Qiagen	Cat#74134
iScript cDNA Synthesis Kit	Bio-Rad	Cat#170–8891
SYBR Green Supermix	Bio-Rad	Cat#1798880
Mm_Actb_1_SG QuantiTect Primer Assay	Qiagen	Cat#QT00095242
Click-iT™ EdU Cell Proliferation Kit for Imaging, Alexa Fluor™ 488 dye	Thermo-Fisher Scientific	Cat#C10337
RNAScope® Multiplex Fluorescent V2 Assay	AdvancedCell Diagnostics, Biotechne	Cat#323136
Neural Tissue Dissociation kit	Miltenyi Biotec	Cat#130- 092-628
CD31 MicroBeads	Miltenyi Biotec	Cat#130-097-418
Chromium Single Cell 3' Reagent Kits v3.1	10x Genomics	Cat#1000121
Deposited data		
scRNAseq from Alk5^{flox} and Alk5iEKO P6 and P10 retinas	NCBI's Gene Expression Omnibus	GSE175895
Experimental models: organisms/strains		
Mouse strain Alk5^{flox}	Larsson et al., 2001	MGI: J:68770
Mouse strain Smad2^{flox}	Ju et al., 2006	MGI: J:119642
Mouse strain Smad3^{flox}	Li et al., 2008	Dr Martin M. Matzuk
Mouse strain Smad4^{flox}	Yang et al., 2002	MGI: J:75140
Mouse strain β-Catenin$^{flox(ex3)}$	Harada et al., 1999	MGI:1858008
Mouse strain mT/mG	Muzumdar et al., 2007	MGI: 3716464
Mouse strain Cdh5CreER^{T2}	Wang et al., 2010	MGI: 3848982
Mouse strain R26CreER^{T2}	Ventura et al., 2007	J: 118233
Mouse strain Mfsd2aCreER^{T2}	Pu et al., 2018	MGI: 5909986
Oligonucleotides		
Alk5 forward primer (QRT-PCR): CGCCCTTTCATTTCAGAGGG		N/A
Alk5 reverse primer (QRT-PCR): CAATTGTTCTTTGAACAAGC		N/A
Cre primer frw (PCR): AAT CTC CCA CCG TCA GTA CG		N/A
Cre primer rev (PCR): CGT TTT CTG AGC ATA CCT GGA		N/A
Alk5flox primer frw (PCR): ACC CTC TCA CTC TTC CTG AGT		N/A
Alk5flox primer rev1 (PCR): ATG AGT TAT TAG AAG TTG TTT		N/A
Alk5flox primer rev2 (PCR): GGA ACT GGG AAA GGA GAT AAC		N/A
mTmG primer frw (PCR): CTC TGC TGC CTC CTG GCT TCT		N/A

REAGENT or RESOURCE	SOURCE	IDENTIFIER
mTmG primer rev1 (PCR): TCA ATG GGC GGG GGT CGT T		N/A
mTmG primer rev1 (PCR): CGA GGC GGA TCA CAA GCA ATA		N/A
β-Cat WT frw (PCR): GGT AGG TGA AGC TCA GCG CAG AGC		N/A
β-cat WT rev (PCR): ACG TGT GGC AAG TTC CGC GTC ATC C		N/A
β-cat GOF forw (PCR): GGT AGT GGT CCC TGC CCT TGA CAC		N/A
β-cat GOF rev (PCR): CTA AGC TTG GCT GGA CGT AAA CTC		N/A
Smad2 flox frw (PCR): AGC TTG AGA AAG CCA TCA CC		N/A
Smad2 flox rev (PCR): GAC CAA GGC GAA AGG AAA CT		N/A
Smad3 flox frw (PCR): CTCCAGATCGT GGGCATACAGC		N/A
Smad3 flox rev (PCR): GGTCACAGGG TCCTCTGTGCC		N/A
Smad4 flox frw (PCR): CAG AGT GGG TCT TTC TAC CTT AGT		N/A
Smad4 flox rev (PCR): CAA GCT TTG AGA ATG TCT GTG ATA G		N/A
Tgfβr1 probe (RNAscope ISH)	AdvancedCell Diagnostics, Biotechne	#406201
Software and algorithms		
Prism 9	Graph Pad	https://www.graphpad.com/scientific-software/prism/
Illustrator	Adobe	https://www.adobe.com
Fiji	https://fiji.sc	Schindelin et al., 2012
Office 365 16.49	Microsoft	https://www.microsoft.com/en-us/microsoft-365/microsoft-office
Photoshop 22.00	Adobe	https://www.adobe.com
CellRanger; version 2.2.0	10x Genomics	RRID:SCR_017344
R; version 3.6.0	https://www.r-project.org/	RRID:SCR_001905
Python; version 3.8.2	https://www.python.org/	RRID:SCR_008394
Emptydrops (DropletUtils package; version 1.6.1)	(Lun et al., 2019)	10.18129/B9.bioc.DropletUtils
Solo; version 0.5	(Bernstein et al., 2020)	https://github.com/calico/solo
Seurat; version 3.2.3	(Stuart et al., 2019)	RRID:SCR_007322
GSVA; version 1.34.0	(Hanzelmann et al., 2013)	RRID:SCR_021058
Other		
Animal chamber with ProOx 110 Compact O2 Controller	BioSpherix, Ltd., Parish, NY	https://biospherix.com/proox-110-2/
Zeiss Laser Scanning Microscope 770	Zeiss	https://www.zeiss.com/microscopy/us/products/confocal-microscopes.html
Zeiss Laser Scanning Microscope 800	Zeiss	https://www.zeiss.com/microscopy/us/products/confocal-microscopes.html